

ОБЪЕДИНЕННЫЙ ИНСТИТУТ ЯДЕРНЫХ ИССЛЕДОВАНИЙ JOINT INSTITUTE FOR NUCLEAR RESEARCH

3[66]-94

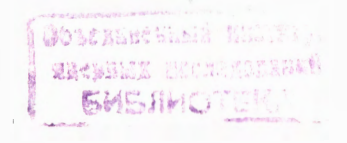
JINR RAPID COMMUNICATIONS

## Объединенный институт ядерных исследований Joint Institute for Nuclear Research

3[66]-94

# JINR RAPID COMMUNICATIONS

сборник collection



## ОГЛАВЛЕНИЕ CONTENTS

S.V.Afanasiev, Yu.S.Anisimov, Yu.N.Gotra, V.N.Jejer,

V.I.Kolesnikov, V.V.Kushpil, A.I.Malakhov, N.A.Malakhov, S.G.Reznikov, P.I.Zarubin	
MRS Silicon Avalanche Detectors with Negative Feedback	
for Time-of-Flight Systems	
С.В.Афанасьев, Ю.С.Анисимов, Ю.Н.Готра, В.Н.Жежер, В.И.Колесников, В.В.Кушпиль, А.И.Малахов, Н.А.Малахов, С.Г.Резников, П.И.Зарубин	
Кремниевые лавинные МРП-детекторы	
с отрицательной обратной связью	
для времяпролетных систем	5
M.Lewitowicz, R.Anne, G.Auger, D.Bazin, J.M.Corre, R.Hue, M.G.Saint-Laurent, R.Grzywacz, M.Pfützner, K.Rykaczewski, J.Żylicz, A.Fomichev, S.Lukyanov, Yu. Penionzhkevich, O.Tarasov, V.Borrel, D.Guillemaud-Mueller, A.C.Mueller, F.Pougheon, O.Sorlin, C.Borcea, Z.Janas, H.Keller, K.Schmidt, T.Dörfler, W.D.Schmidt-Ott, M.Huyse, J.Szerypo, J.Wouters Identification of the Doubly-Magic Nucleus 100 Sn in the Reaction 112 Sn(63 MeV/Nucleon) + nat Ni M.Левитович, Р.Анн, Г.Оже, Д.Базин, Дж.Корр, Р.Хью, М.Г.Сэн-Лоран, Р.Грживач, М.Пфюцнер, К.Рикачевский, Дж.Зилич, А.Фомичев, С.Лукьянов, Ю.Пенионжкевич, О.Тарасов, В.Боррель, Д.Гюльмо-Мюллер, А.С.Мюллер, Ф.Пужо, О.Сорлин, К.Борча, З.Янас, Х.Келлер, К.Шмидт, Т.Дерфлер, В.Д.Шмидт-Отт, М.Хайс, Дж.Шерипо, Дж.Ваутерс Идентификация дважды магического ядра	
в реакции <sup>112</sup> Sn(63 МэВ/нуклон) + <sup>nat</sup> Ni	11
M.G.Itkis, Yu.Ts.Oganessian, G.Chubarian, V.V.Pashkevich, V.S.Salamatin, A.Ya.Rusanov, V.N.Okolovich, G.N.Smirenkin Multimodal Fission of Neutron-Deficient Nuclides of Th and Ac М.Г.Иткис, Ю.Ц.Оганесян, Г.Чубарян, В.В.Пашкевич, В.С.Саламатин, А.Я.Русанов, В.Н.Околович, Г.Н.Смиренкин Мультимодальное деление	
нейтронолефицианых нуклилов Тh и Ac	19

И.В.Кузнецов, М.П.Иванов, В.Ф.Кушнирук, Ю.Г.Соболев,
Г.В.Букланов
Инклюзивные энергетические спектры
легких заряженных частиц (p, d, t, <sup>4</sup> He)
в спонтанном делении <sup>248</sup> Cm
I.V.Kuznetzov, M.P.Ivanov, V.F.Kushniruk, Yu.G.Sobolev,
G.V.Buklanov
The Inclusive Energy Spectra
of Light Charged Particles (p, d, t, <sup>4</sup> He) from Spontaneous Fission of <sup>248</sup> Cm
from Spontaneous Fission of <sup>248</sup> Cm
M.K.Gaidarov, A.N.Antonov, S.S.Dimitrova, M.V.Stoitsov
Nucleon Correlation Effects on Y-Scaling Quantities in Nuclei
М.К.Гайдаров, А.Н.Антонов, С.С.Димитрова, М.В.Стоицов
Нуклонные корреляционные эффекты
на У-скейлинговых величинах в ядрах

### MRS SILICON AVALANCHE DETECTORS WITH NEGATIVE FEEDBACK FOR TIME-OF-FLIGHT SYSTEMS

S.V.Afanasiev, Yu.S.Anisimov, Yu.N.Gotra, V.N.Jejer, V.I.Kolesnikov, V.V.Kushpil, A.I.Malakhov, N.A.Malakhov, S.G.Reznikov, P.I.Zarubin

Investigation of time characteristics of Metal-Resistive layer-Semiconductor structure based silicon avalanche detectors with negative feedback, proposed for time-of-flight, is described. Time resolutions of 550 ps on  $\beta$ -electrons and 250 ps on LED light pulses were obtained. Design and principles of operation are described briefly.

The investigation has been performed at the Laboratory of High Energies, JINR. Results were presented at SPHERE collaboration workshop, Varna, Bulgaria, May 31 — June 5, 1994.

Кремниевые лавинные МРП-детекторы с отрицательной обратной связью для времяпролетных систем

## С.В.Афанасьев и др.

Описаны исследования временных характеристик кремниевых лавинных детекторов на основе структуры металл-разистивный слой-полупроводник с отрицательной обратной связью, предлагаемых для в ремяпролетных систем. Получено временное разрешение 550 пс на  $\beta$ -электронах и 250 пс на световых импульсах от светодиода. Также приводится краткое описание конструкции и принципа работы детектора.

Работа выполнена в ЛВЭ ОИЯИ. Результаты были представлены на Рабочем совещании коллаборации «СФЕРА», проходившем в Варне (Болгария) 31 мая — 5 июня 1994 г.

### Introduction

The present and future experiments in high energy and nuclear physics require detectors for the time-of-flight systems with high time resolution. There are few ways to solve this problem: using phototubes and scintillators or silicon avalanche detectors of different designs. But phototubes and scintillators require high voltage supply and large enough volume. Silicon avalanche diodes with p-i-n structure are compact but also require high voltage supply (300—2000 V) [1].

An additional way to solve this problem is the silicon avalanche detectors with a negative feedback [2–4]. Produced on low-resistivity substrate they are cheaper than avalanche detectors on high-resistivity silicon. These detectors operate at low voltages (about 40 V) and at room temperatures. Due to high gain of these detectors  $(10^3 - 10^5)$  it is possible to obtain good signal-to-noise ratio collecting charge carriers from the active layer  $2 \,\mu \text{m}$  thick. Due to thin depletion layer it may be possible to collect charge carriers for a time about 100 ps or less. The main problem here is high intrinsic capacitance of the detector that makes high RC constant of detectors.

In this paper we describe the design and principles of operation of the detector and present some results of time characteristic measurements.

## 1. Silicon Avalanche Detectors with Negative Feedback

Silicon avalanche detectors with negative feedback (SiAD) were designed and produced by INR (Troitsk) group in collaboration with MELZ (Moscow) [2—4] and some detectors were produced at the Institute for Electronics of Byelorussian Academy of Sciences (Minsk). They are made on the low resistivity (1  $\Omega \cdot$  cm) p-type silicon substrate 300  $\mu$ m thick and have Ni-SiC-Si-Al structure. Schematically the structure of the detector is presented in Figure 1. The thickness of SiC layer is 0.2—0.5  $\mu$ m. Application of bias voltage of only 37—42 V allows one to reach, in the region near the SiC-Si boundary, electric field more than 3·10<sup>5</sup> V/cm that is enough for impact ionization.

A minimum ionizing particle (e.g., relativistic electron) creates in space charge region (depletion layer) about 100 electron-hole pairs. Due to avalanche amplification  $(10^3+10^5)$  we can collect charge carriers on a

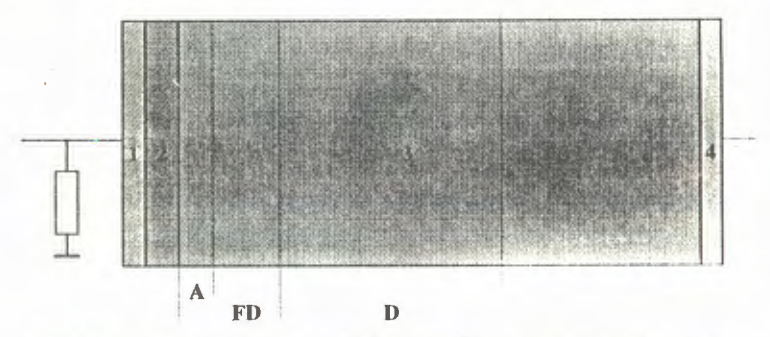


Fig.1. Simplified structure of the MRS detector: 1 - Ni; 2 - SiC; 3 - p-Si; 4 - Ai; A - avalanche region, FD - full depletion layer, D - diffusion layer

readout electrode  $10^5+10^7$ . It is compatible (or even two orders more) with conventional silicon detectors (without avalanche amplification — about  $3\cdot 10^4$  carriers for minimum ionizing particle). So more simple electronics may be used for such charge registration.

The avalanche occurs immediately after the incident particle passes through the avalanche multiplication region. Redistribution of the bias in the MRS structure and partial charge accumulation at the Si-SiC boundary takes place during the avalanche. Due to these processes the electric field at the avalanche multiplication region is decreased and it results in the self-stabilized avalanche process. So a local negative feedback occurs between the avalanche process rate and the potential drop across the resistive layer [4]. The working surface of the detector is covered by thin Ni film to provide optical transparency since these detectors originally were designed for light quanta registration.

Because these detectors are produced on low-resistivity p-type silicon it is possible to make detector and amplifiers on the same wafer. They also can be used as position sensitive devices, e.g., pixel or microstrip detectors with or without electronics on the wafer.

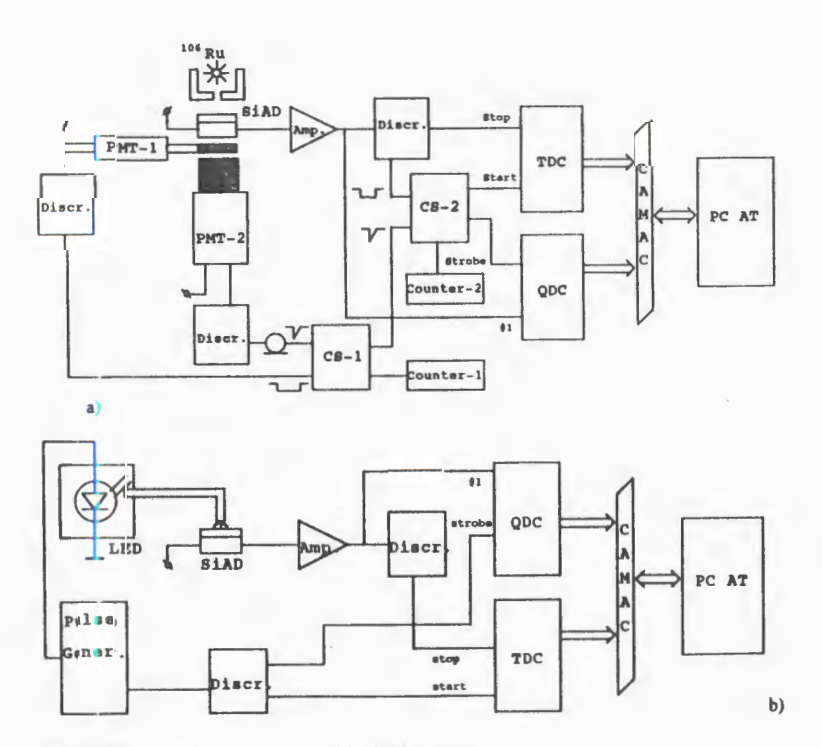
#### 2. The Time Resolution Measurements

First result of the SiAD time resolution measurement was obtained in November 1993 with square detector of area 5×5 mm<sup>2</sup> produced by MELZ [5].

The silicon avalanche detector had been exposed to beta electrons from a source which has an end point energy of 3.5 MeV. The particles were collimated, passed through SiAD and two triggering scintillators with PMTs. The triple coincidence from SiAD and scintillators were used to trigger an event. The schematic diagram of the experimental setup is shown in Figure 2a. The gain of preamplifier was 7.

The resolution of the detector  $\sigma=630$  ps was measured. But this result was obtained using a simple custom designed preamplifier. The time spectrum of this detector is presented in Figure 3.

The same measurements were performed with a circular SiAD with diameter 3 mm (area 7 mm²). A PHILIPS Scientific Pulse Preamplifier Model 6954 ( $K_u \approx 20$ ,  $\tau_{\rm rise} = 180$ , bandwidth 2 GHz) was used in these tests. Time resolution was obtained to be  $\sigma = 550$  ps (Figure 4a). The time resolution of the detectors seems to be area-independent (detectors with 25 mm² and 7 mm² areas differ more than 3 times) but it is slightly difficult to compare these results because amplifier with different time characteristics



 $Fig. 2 \ \ The \ measurement \ set-up \ block \ diagram:$ 

- a) with  $\beta$ -source; b) with LED.
- QDC charge-to-digit converter; TDC time-to-digit converter;
- CS coincidence scheme; Amp. amplifier; Discr. discriminator

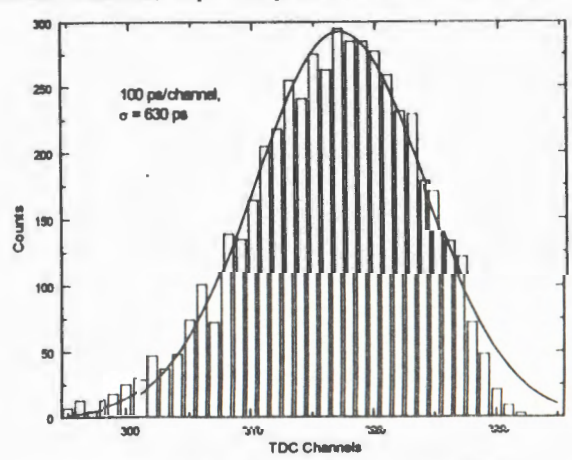


Fig. 3. Time spectrum of the  $5\times 5~\text{mm}^2$  detector from  $^{106}\text{Ru}$   $\beta$ -source.

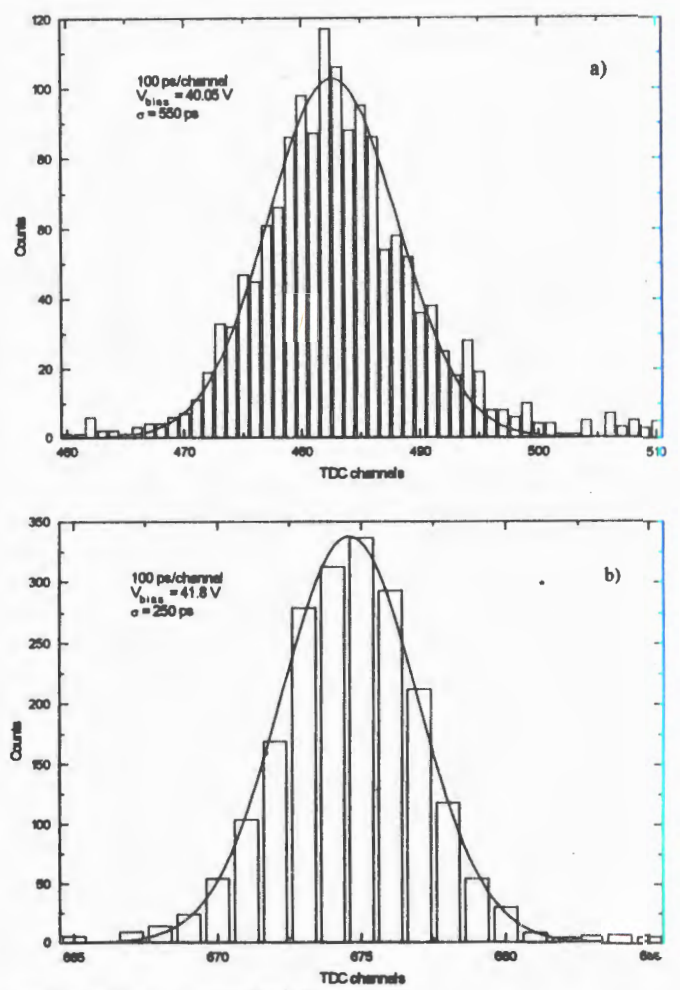


Fig. 4. The 3 mm diameter SiAD time spectra: a) with  $^{106}{\rm Ru}\,\beta\text{-source};$  b) with LED (y = 610+780 nm)

were used and the detectors were produced by different enterprises, production conditions of which might differ.

Next test was with light pulses from an LED to study the possibility of improving the detector time parameters. The measured time resolution is  $\sigma = 250$  ps (Figure 4b).

The test consisted of exposing the SiAD to LED light pulses with a wavelength 610+780 nm. The LED was supplied with orthogonal pulse generator

(pulse height is 50—100 V, risetime about 100 ps). Strobe signals of the generator were used as TDC «start» and the SiAD signals were used as «stop». Block diagram of the measurement set-up is shown in Figure 2b.

## 3. Work in Progress and Further Plans

Further theoretical considerations let us to conclude that better results may be obtained with modification and optimization of the avalanche detectors for time measurements purpose. Simulation of the detector parameters is in progress now to better understand principles of operation of the detector and optimize the parameters. We plan to investigate different types of the silicon avalanche detectors with negative feedback to obtain the best results. One of the possible ways to improve the detector characteristics is using more pure silicon substrate with more uniform and smooth surface. Also the radiation hardness of them is a subject for studying.

## Acknowledgments

We would like to thank Z.Y.Sadygov of Physics Institute of Azerbaijan Academy of Scienses, G.A.Sokol of Lebedev Physics Institute of Russian Academy of Sciences and V.B.Zalessky of Institute for Electronics of Byelorussian Academy of Sciences for samples of detectors and consultations during the investigation, and Dr. A.Rudge of CERN for the fast preamplifier and interest to this research. And special thanks to Academician A.M.Baldin, Director of the Laboratory of High Energies, JINR and A.D.Kovalenko, Head of engineer staff of the LHE, JINR for their support of our research program.

#### References

- 1. Hauger A. et al. IEEE Trans. on Nucl. Sci., 1993, pp.242-244.
- 2. Gasanov A.G. et al. Preprint INR P-0673, 1990 (in Russian).
- 3. Govorkov B.B. et al. Preprint of Lebedev Physical Institute No.14, 1993.
- 4. Kirillova T.A. et al. Preprint INR-836/93, November, 1993.
- 5. Afanasiev S.V. et al. ALICE/93-35 Internal Note/PHS, 22 November, 1993.

Received by Publishing Department on July 21, 1994.

## IDENTIFICATION OF THE DOUBLY-MAGIC NUCLEUS $^{100}$ Sn IN THE REACTION $^{112}$ Sn(63 MeV/NUCLEON) + $^{nat}$ Ni

M.Lewitowicz, R.Anne, G.Auger, D.Bazin, J.M.Corre, R.Hue, M.G.Saint-Laurent GANIL, BP 5027, 14021 Caen Cedex, France

R.Grzywacz, M.Pfutzner, K.Rykaczewski, J.Żylicz IFD, Warsaw University, 00681 Warsaw, Poland

A.Fomichev, S.Lukyanov, Yu. Penionzhkevich, O.Tarasov FLNR, JINR, 141980 Dubna, Moscow region, Russia

V.Borrel, D.Guillemaud-Mueller, A.C.Mueller, F.Pougheon, O.Sorlin IPN, 91406, Orsay Cedex, France

C.Borcea

IAP, Bucharest-Magurele P.O.Box MG6, Roumania

Z.Janas<sup>1</sup>, H.Keller, K.Schmidt GSI, Postfach 110552, D-64220, Darmstadt, Germany

T.Dörfler, W.D.Schmidt-Ott University of Göttingen, D.3400, Göttingen, Germany

M.Huyse, J.Szerypo<sup>1</sup>, J.Wouters IKS KU, B-3001, Leuven, Belgium

We report on the production of the doubly-magic nucleus  $^{100}$ Sn and other proton-rich nuclei in the A = 100 region in the reaction  $^{112}$ Sn +  $^{nat}$ Ni at 63 MeV/nucleon. The experiment was carried out using the high acceptance device SISSI and the Alpha and LISE3 spectrometers at GANIL. The identification of the reaction products (A, Z and Q) was made using the measurements of time-of-flight, energy-loss and kinetic energy.

The investigation has been performed by an international collaboration of scientists from FLNR, JINR (Dubna), GANIL (Caen), Warsaw University, IPN (Orsay).

Идентификация дважды магического ядра  $^{100}$ Sn в реакции  $^{112}$ Sn (63 МэВ/нуклон) +  $^{\rm nat}$ Ni

М.Левитович и др.

Представлены результаты по получению дважды магического ядра  $^{100}$ Sn и других протонно-обогащенных ядер в области A=100 в реакции  $^{112}$ Sn(63 MэB/A +  $^{nat}$ Ni). Эксперимент проводился с использованием ус-

On leave of absence from IFD, Warsaw University, 00681 Warsaw, Poland

тановки с высоким акцептансом SISSI и спектрометров ALPHA и LISE3 (GANIL). Идентификация продуктов реакции по A, Z и Q проводилась путем измерения их времени пролета, потерь энергии и кинетических энергий.

Работа выполнена в международном сотрудничестве ученых из ФЛЯР ОИЯИ (Дубна), ГАНИЛ (Кан), Университет (Варшава), ИЯФ (Орсе).

#### 1. Introduction

Studies of N=Z and neighbouring nuclei, especially in the region of a double shell closure, are important for the tasting and further development of nuclear models [1,2]. In particular, these studies provide information about the interaction between protons and neutrons occupying the same shell-model orbits.

While N=Z nuclides of low mass are mostly stable, the heavier ones lie away from the line of beta stability. In the case of  $^{100}$ Sn, the deficit of neutrons with respect to the mean atomic mass of the stable tin isotopes is about 18 and it is expected [3] to be the heaviest N=Z nuclear stable against ground-state proton decay. This stability is related to the doubly-magic character of  $^{100}$ Sn. It may be noted that for heavier N=Z nuclei the condition of double shell closure is not sufficient to ensure stability:  $^{164}$ Pb presumably lies well beyond the proton drip line. Mapping the proton-drip line in the neighbourhood of  $^{100}$ Sn may also be of great importance in an astrophysical context as the properties of the proton-rich nuclei dictate the pathway of the rapid proton capture process in hot, dense stellar environments [4].

Beta decay in the  $^{100}$ Sn region can be described in a very simple shell-model picture. It is strongly dominated by one channel, the  $\pi g_{9/2} \rightarrow \nu g_{7/2}$  Gamow-Teller (GT) transition, and thus the observation of fast beta decays can lead to the unambiguous identification of the parent and daughter nuclear states. A meaningful verification of model predictions can be performed as, due to the high  $Q_{EC}$  values, the beta decay strength can be determined over a large energy range [5]. This had been a motivation for a series of experiments using on-line mass separators at GSI Darmstadt, LLN IKS Leuven and CERN/ISOLDE Geneva [1].

The nuclei  $^{100}$ In  $(T_{1/2} = 5 \pm 1 \text{ s})$  and  $^{101}$ Sn are the closest ones to  $^{100}$ Sn discovered so far using a fusion-evaporation reaction  $(^{58}\text{Ni}(5 \text{ MeV/nucleon}) + ^{50}\text{Cr})$  and the on-line mass-separation technique

[6,7]. These nuclei were identified via the measurement of beta-delayed protons, a decay mode which becomes energetically possible in this region due to the high  $Q_{EC}$ . However, any attempt to produce and identify in the same way  $^{100}\mathrm{Sn}$  is most probably hopeless. Indeed, for  $^{101}\mathrm{Sn}$  approximately one proton was observed per hour, for the proton branching ratio that is predicted to be larger than 10%. The production rate and the proton branching ratio in the case of  $^{100}\mathrm{Sn}$  are expected to be at least one and several orders of magnitude lower respectively. Obviously other production methods and identification techniques have to be used to reach and study  $^{100}\mathrm{Sn}$  [8]. The expected increase of the production yields is mainly due to the use of  $^{112}\mathrm{Sn}$  as a projectile. This rare primary beam is developed at GANIL in a close and already very fruitful collaboration with the Laboratory of Nuclear Reactions, JINR at Dubna.

Recently, in April 1994, <sup>100</sup>Sn was identified in projectile-fragment separator based experiments. In this letter we report on the work performed at GANIL using a 63 MeV/nucleon <sup>112</sup>Sn beam [9,10]. The experiment carried out at GSI with a 1.1 GeV/nucleon <sup>124</sup>Xe beam is described in ref. [11].

To produce and identify <sup>100</sup>Sn at GANIL a fragmentation-like reaction was employed in conjunction with the new SISSI device [12] and the magnetic spectrometers Alpha [13] and LISE3 [14] which provided for the collection, separation and in-flight identification of the different reaction products. In order to enhance the production of neutron-deficient isotopes a beam of the lightest, stable tin isotope, 112Sn, and a natural Ni target (68.3% <sup>58</sup>Ni) were used. In an earlier experiment [9], we had already observed the neutron deficient tin isotopes down to <sup>101</sup>Sn, including the previously unknown <sup>102</sup>Sn. In addition, new isotopes of rhodium (<sup>92</sup>Rh, <sup>93</sup>Rh) and palladium (93Pd) were clearly observed and evidence for the production of even lighter isotopes of these elements, such as 91Rh, 90Rh, 89Rh and 92Pd, was also obtained (identification of these neutron-deficient rhodium and palladium isotopes has been very recently reported by a group working at MSU [15]). The present experiment, performed with a substantially enhanced experimental arrangement provided a confirmation of these results and the discovery of several new nuclides, including 100Sn. Here we present the evidence for <sup>100</sup>Sn while the entire data set (e.g. the evidence for

 $^{105}\mathrm{Sb}$  and the new isotope  $^{104}\mathrm{Sb}$ ) will be the subject of a forthcoming publication.

## 2. Identification of 100 Sn and Neighbouring Nuclei

The experimental set-up for the identification of  $^{100}$ Sn and neighbouring nuclei is shown in figure 1. The production target was located between the two superconducting solenoids of SISSI. Thus, in comparison with the previous experiment [9] the angular acceptance for the reaction products was increased by an order of magnitude and the flight-path (118m in the present experiment) increased by almost a factor of 3. The momentum analysis was performed using the Alpha spectrometer  $(B\rho = 1.876 \, \text{Tm})$  with an acceptance  $\Delta p/p = \pm 0.29\%$ .

To reduce the rate of the light, fully stripped fragments arriving at the final focus of LISE3 with  $A/Z \approx 2$ , a thin mylar foil (1.5 $\mu$ m) was placed at

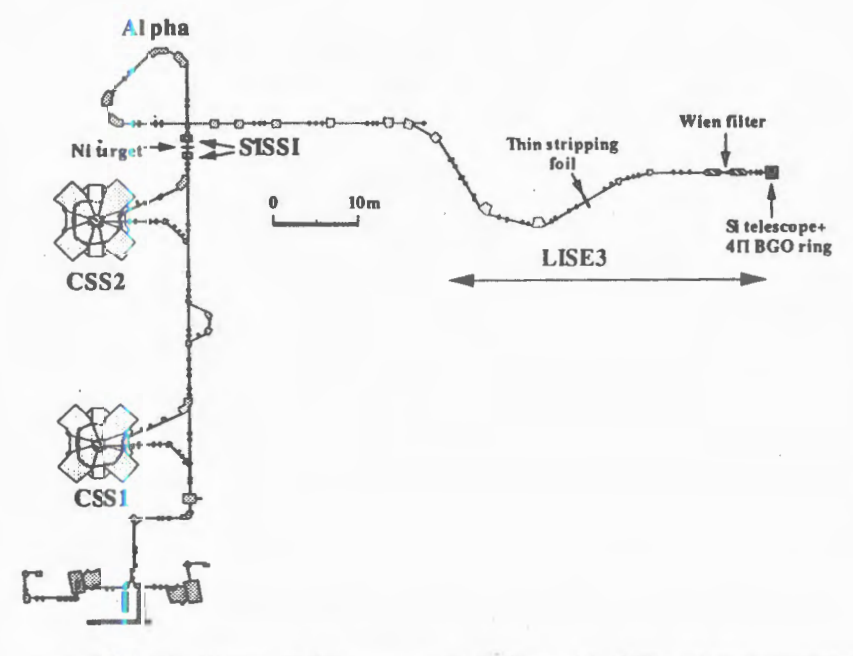


Fig.1. Schematic diagram of the experimental facilities at GANIL used to produce and identify  $^{100}\mathrm{S}\,\mathrm{n}$ 

the intermediate focal plane (see figure 1). The function of this foil was to change the charge state distributions of the heavy fragments without modifying the velocities. For example,  $^{100}\mathrm{Sn}^{+48}$  was converted into a mixture of  $^{100}\mathrm{Sn}^{+49}$ ,  $^{100}\mathrm{Sn}^{+48}$  and  $^{100}\mathrm{Sn}^{+47}$  (the charge state Q=+48 was the most strongly populated after the target and stripping foil for the tin isotopes). Light fragments, however, remained fully stripped. Consequently, by employing an acceptance range in the second section of LISE3 from  $1.013 \times B\rho$  to  $1.063 \times B\rho$ , the transmission of fully stripped ions was strongly suppressed and that of the nuclei in the region of interest was favoured. The number of unwanted particles was further reduced using the velocity filter located at the end of LISE3.

Fragments arriving at the final focus of LISE3 were stopped in a telescope consisting of four silicon detectors:  $E1(300\mu\text{m})$ ,  $E2(300\mu\text{m})$ ,  $E3(300\mu\text{m})$  and  $E4(500\mu\text{m})$ . Since ions in the mass region of interest were stopped in the E2 detector, the E1 detector provided information on the energy-loss ( $\Delta E$ ), while the E1 and E2 detectors combined served to determine the total kinetic energy (TKE). The E3 and E4 detectors were used in veto to reject events corresponding to lighter ions. The time-of-flight (TOF) was measured using a start signal provided by the first Si detector (E1) and a stop signal derived from the radio-frequency of the second cyclotron. Finally, a segmented BGO ring [16] surrounding the implantation telescope was used for the detection of prompt gamma-rays in order to reject events corresponding to reactions in the detectors.

The Ni target (144 mg/cm<sup>2</sup>) was mounted such that the angle with respect to the beam axis could be changed from 0° to 45°. Anglesi between 36° and 45° were used to allow the transmission of  $^{112}$ Sn ions with Q=+46 to +50 to the Si detector telescope in order to provide calibrations for the energy-loss, total kinetic energy and time-of-flight measurements. It should be noted that the magnetic rigidity of the beam line from the production target to the stripping foil remained fixed during the whole experiment at 1.876 Tm. This corresponded to the maximum calculated production rate for  $^{100}$ Sn  $^{+48}$  ions.

The transmission of the beam line from the exit of the Alpha spectrometer to the final focus of LISE3 was measured using movable  $300\,\mu\text{m}$  Si detectors located at the exit of the Alpha spectrometer, at the entrance to and at the intermediate focal plane of LISE3 and using the Si detector telescope. A transmission of nearly 100% was found.

The resolution (FWHM) of the TOF measurement was about 1 ns, while the TOF ranged from 1.4 to 1.5  $\mu$ s. The atomic number of the fragments (Z) was calculated using the  $\Delta E$  measured with E1 detector and absolute Z

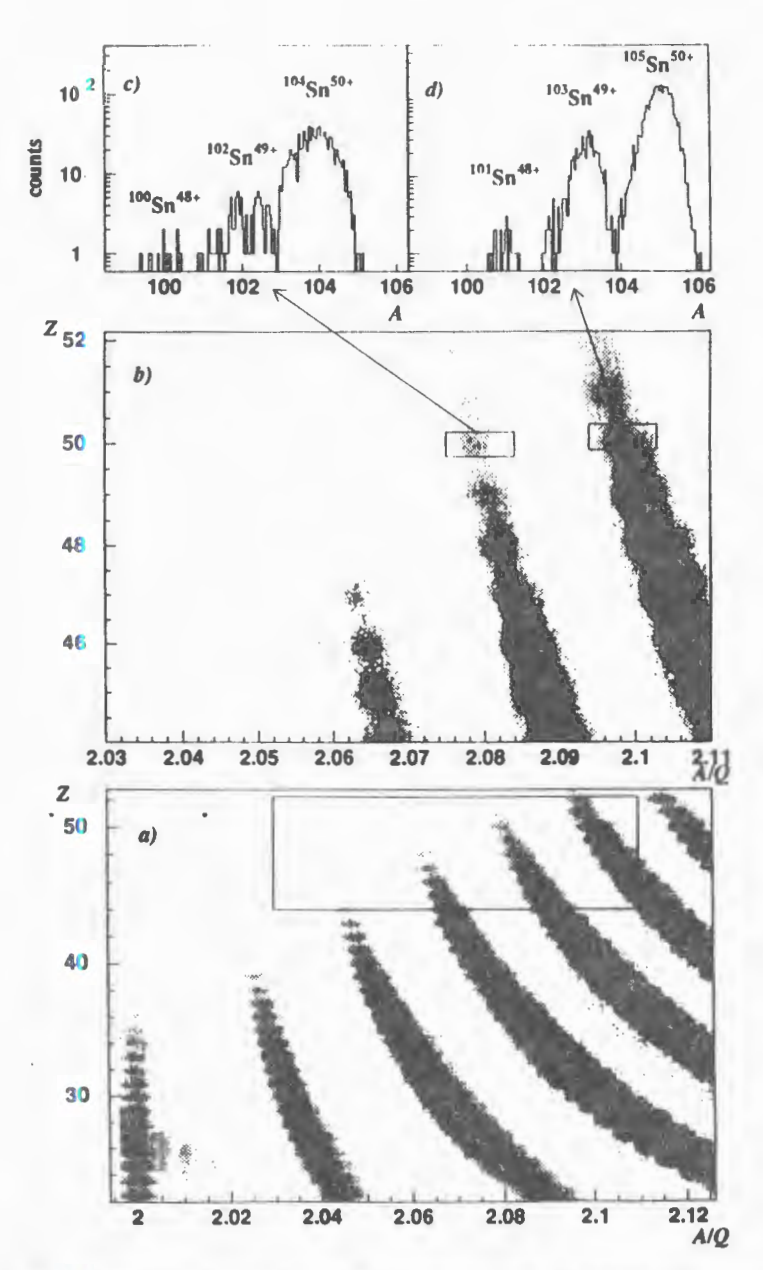


Fig. 2. Identification of the reaction products: a) atomic number (Z) versus mass-to-charge ratio (A/Q); b) region of plot a) with two groups of tin isotopes indicated for which mass (A) distributions have been calculated as shown in planels c) and d). The charge states indicated correspond to those before the stripping foil (see text)

identification was obtained from the charge states of  $^{112}$ Sn primary beam [9]. Another unambiguous assignment of the Z was obtained from the direct identification of the light ions in the  $\Delta E$  versus TOF spectrum. In figures 2a and b the mass to charge ratio, A/Q, determined from the  $B\rho$  and measured TOF is displayed versus Z for the nuclei in the region of interest.

It is possible to calculate for a group of events selected on the basis of the Z and A/Q (figure 2), the masses of the individual ions from the measured TKE and TOF [9]. The resulting mass distributions for  $^{104}\mathrm{Sn}^{+50}$ ,  $^{102}\mathrm{Sn}^{+49}$ ,  $^{100}\mathrm{Sn}^{+48}$  and  $^{105}\mathrm{Sn}^{+50}$ ,  $^{103}\mathrm{Sn}^{+49}$ ,  $^{101}\mathrm{Sn}^{+48}$  are given in figures  $^{2c}$  and  $^{2c}$  respectively. Eleven events corresponding to  $^{100}\mathrm{Sn}^{+48}$  were observed over a period of 44 hours a primary beam intensity of  $^{2c}$  pnA. The relative yields of the different isotopes of tin shown in figure 2 do not reflect the corresponding production cross-sections as they are affected by the distribution of the products over the different charge states as well as the different transmission efficiencies.

The number of events observed may be used to obtained a lower limit for the production cross-section by taking into account the estimated transmission efficiency (~5%) and the charge state distribution measured for the  $^{112}$ Sn beam after the Ni target. For  $^{100}$ Sn this leads to  $\sigma \ge 120$  pb.

At present, the time correlations for 511—511 keV gamma-ray pairs recorded in opposite segments of the BGO ring, in coincidence with heavy fragments implanted in the telescope, have not been analyzed. However, the production rates are promising for future half-life and mass measurements.

## 3. Summary

For the first time nuclei near and at the proton drip-line in the region of the doubly-magic nucleus  $^{100}$ Sn have been produced with relatively high rates — about 5 per day for  $^{100}$ Sn. This result confirms that medium energy fragmentation-like reactions combined with projectile-fragment separation techniques presently offer the most efficient method for the production of very neutron-deficient nuclei up to  $A \approx 100$ .

As a much higher intensity primary beam and a larger momentum acceptance for the Alpha spectrometer are available; an increase in the production rate of <sup>100</sup>Sn by at least a factor of 5 seems feasible.

The authors wish to acknowledge the efforts of the cyclotron staff and technical support of GANIL. We also thank Nigel Orr for assistance in the preparation of the manuscript.

#### References

- 1. Rykaczewski K. Proc. of 6th Int. Conf. on Nuclei far from Stability and 9th Int. Conf. on Atomic Masses and Fundamental Constants, Bernkastel-Kues 1992, R.Neufarth, A.Wohr (eds), IOP Conf. Ser., 1993, 132, p.517.
- 2. Johnson A. et al. Nucl. Phys., 1993, A557, p.401c.
- 3. Haustein P.E. (ed.) At. Data Nucl. Data Tables, 1988, 39, p.185.
- 4. Wallace R.K., Woosley S.E. Astrophys.J.Suppl., 1981, 45, p.389.
- 5. Brown B.A., Rykaczewski, sumbitted to Phys.Rev.Lett.
- 6. Szerypo J. et al, to be published.
- 7. Roeckl E. CSI-Nachrichten, 1993, 09-93, p.3.
- 8. Anne R. et al., "Towards the Study of Gamow-Teller Beta Decay of <sup>100</sup>Sn, proposal to the GANIL Comite d'Experiences, June 1993, Ganil Report 93 06, p.70.
- 9. Lewitowicz M. et al. Nouvelles de Ganil, 1993, 48, p.7.
- 10. Lewitowicz M. et al. Nouvelles de Ganil, 1994, 50, p.3.
- 11. Schneider R. et al., submitted to Z.Phys.A.
- 12. Joubert A. et al. Proc. of the Second Conf. of the IEEE Particle Accelerator, San Francisco, May 1991, p.594 and SISSI, Nuclear Physics News. 1990, vol.1, №2, p.30.
- 13. Rebmeister R. et al. Report CRN/PN 1983-16, 1983.
- 14. Anne R, Mueller A.C. Nucl. Instr. and Meth., 1992, B70, p.276.
- 15. Hencheck M. et al., submitted to Phys. Rev. C as Brief Report.
- 16. Keller H. et al. Z. Phys. A, 1991, 340, p.363.

## MULTIMODAL FISSION OF NEUTRON-DEFICIENT NUCLIDES OF Th AND Ac

M.G.Itkis, Yu.Ts.Oganessian, G.Chubarian, V.V.Pashkevich<sup>1</sup>, V.S.Salamatin, A.Ya.Rusanov<sup>2</sup>, V.N.Okolovich<sup>2</sup>, G.N.Smirenkin<sup>2</sup>

Investigations of low-energy fission in reactions  $^{204,208}$ Pb and  $^{203}$ Tl +  $^{16}$ O have been performed with the help of the double-arm time-of-flight fragment spectrometer on the U-400 cyclotron beam, FLNR, JINR. The goal is to obtain experimental information on multimodal structure of mass-energy fragment distributions in the field of A fissionable nuclei earlier unstudied. For the first time, with such purpose heavy ion-induced reactions have been used. In connection with the experimental data obtained the influence of nuclein nuclei composition on principal fission modes — symmetric and asymmetric ones  $(Y_3/Y_4)$  — are discussed.

The investigation has been performed at the Flerov Laboratory of  $\ensuremath{\text{Nuclear}}$  Reactions, JINR.

Мультимодальное деление нейтронодефицитных нуклидов Th и Ac

М.Г.Иткис и др.

На пучке циклотрона У-400 ЛЯР им.Г.Н. Флерова (ОИЯИ) с помощью двухплечевого времяпролетного спектрометра осколков проведены исследования низкоэнергетического деления в реакциях <sup>204,208</sup>Pb и <sup>203</sup>Tl + <sup>16</sup>O с целью получения экспериментальной информации о мультимодальном строении массово-энергетических распределений осколков в неизученной ранее области А делящихся ядер. Впервые с такой целью использованы реакции с тяжелыми ионами. В связи с полученными экспериментальными данными обсуждается влияние нуклонного состава ядер на соотношение основных мод деления — симметричной и асимметричной.

Работа выполнена в Лаборатории ядерных реакций им.  $\Gamma$ . Н. Флерова, ОИЯИ.

JINR, Dubna and CENBG, Bordeaux, France

<sup>&</sup>lt;sup>2</sup>Institute of Nuclear Physics, Alma-Ata, Kazakhstan

One of the important results obtained in the fission physics during the last several years is the experimental discovery of multimodal structure of fragment mass and energy distributions of low energy fission nuclei in the region of Pb [1] and of the spontaneous fission of nuclei in the vicinity of Fm [2] as well as the establishing of the genetic relation of this phenomenon with structural (shell) peculiarities of the deformation potential energy surface of a nucleus fissioning along the mass asymmetric coordinate [3].

The unstudied earlier region of transient nuclei between At and Th seems to be rather promising for further investigation of the formation mechanisms of mass, energy and charge distributions of fragments in general and of the multimodal fission in particular. Just in this region one can expect a sharp change in the properties of mass, energy and charge distributions of fission fragments depending on the nucleon composition and excitation energy, i.e., the transition from symmetric to asymmetric fission and related changes in the barrier heights ratio of mass-symmetric and mass-asymmetric fission modes, the length and duration of nucleus motion from the saddle point to the scission point. That is why the experimental data on the character and scale of these changes should be critical for testing the theoretical description of dynamic and static aspects of the fission process.

Unfortunately, the advance into the indicated region of nuclei is hampered by a serious experimental problem caused first of all by the absence of stable nuclides with Z=84-87 which could be used as target nuclei in reactions with light charged particles and neutrons that are traditionally used for the investigation of the fission process at low energies  $E^* \le 20-30$  MeV.

The present study attempts to apply for the discussed purpose reactions with heavy ions. Their research object is usually very neutron deficient nuclides. The main difficulty in the realization of the given possibility is related with the production of nuclei with an excitation energy  $E^* \le 20-30$  MeV which corresponds to the energy of ions near and below the Coulomb barrier  $E_i \le B_c$  and consequently with a rapid decrease of the fission cross section at decreasing  $E_i$  (when decreasing  $E^*$ , one achieves a better separation of fission modes, which is especially important when one of them dominates, as is expected in our case). According to the idea, on which the cold synthesis [4] method is based, the smallest excitation energy on account of the Q-reaction is achieved in the case of using as a target the double magic nuclei near  $^{208}$ Pb and ions of  $^{12}$ C,  $^{16}$ O.

In this connection we have chosen for the first experiments the reaction <sup>208</sup>Pb(<sup>16</sup>O, f) for which the fission cross sections, distribution of <sup>224</sup>Th compound nuclei angular momenta and spectra of pre- and post-neutrons

[5,6] are already known. The two other selected reactions, <sup>204</sup>Pb(<sup>16</sup>O, f) and <sup>203</sup>Tl(<sup>16</sup>O, f) lead to the formation and fission of compound nuclei <sup>220</sup>Th and <sup>219</sup>Ac and along with that satisfy the criterion of minimum excitation energy.

Note that at present the GSI realized another opportunity of studying the low-energy fission of transient nuclei and the use of relativistic secondary beams of radioactive nuclei of the <sup>222</sup>Th, <sup>225</sup>Th type and of their fission in the process of electromagnetic dissociation on an active target [7].

In this research, measurements were performed with a two-arm time-of-flight spectrometer of fragments «DEMAS-2» on the extracted ion beam of the U-400 cyclotron of FLNR, JINR. The spectrometer consists of two wide-aperture position sensitive avalanche counters providing the registration of fragments within the solid angle of about 0.2 steradian for each arm and of start-up parallel-plate avalanche counters [8].

Masses and energies of fragments were deduced from a set of experimentally measured values  $T_{1,2}$  of the time-of-flight and  $X_{1,2}^-$ ,  $Y_{1,2}$  coordinates of reaction products entry into the detector. The two-body processes in this case were selected on the condition  $\overline{\Theta}_1 + \overline{\Theta}_2 = 180^\circ \pm 3^\circ$ , where  $\overline{\Theta}_{1,2}$  are the divergence angles in the center of mass system.

The spectrometer was calibrated by means of a thin source of spontaneous fission fragments of  $^{252}$ Cf and provided the time resolution of about 200 pico sec. and the mass resolution  $\delta M/M \cong 2\%$  (the peak/valley ratio in the mass distribution of  $^{252}$ Cf  $\cong 25$ ). In these experiments there were used targets of enriched isotopes of  $^{204}$ Pb,  $^{208}$ Pb and  $^{203}$ Te with a thickness of  $\cong 150-200\,\mu\text{g/cm}^2$  sputtered on a substrate of  $\text{Al}_2\text{O}_3$  with a thickness of  $30-50\,\mu\text{g/cm}^2$ . The beam intensity and its energy spread were  $\cong 1\times10^{11}$  pps and 0.5%, respectively.

The data on the energy characteristics of reactions investigated and on experimental values of the first momenta of fragments mass and energy distributions are presented in the Table, where  $E_l$ —the ion energy in the laboratory system of coordinates,  $E^*$ —the excitation energy of the complex compound nucleus,  $E_{sp}^*$ —the excitation energy of the fissioning nucleus in the saddle point,  $\langle l^2 \rangle$ —the mean square of the transferred angular momentum [9].  $E_K$ —the average kinetic energy of fragments,  $\sigma_E^2$  and  $\sigma_M^2$ —the fragments energy and mass dispersions. Note that the large

Table

Reaction	Comp.	$E_i$ , MeV	E*, MeV	E <sub>f</sub> MeV	E <sub>sp</sub> , MeV	$\langle l^2 \rangle$ , $h^2$	$\langle E_k \rangle$ , MeV	σ <sub>E</sub> , MeV <sup>2</sup>	o <sub>M</sub> , (amu) <sup>2</sup>
<sup>16</sup> O + <sup>208</sup> Pb	<sup>224</sup> Th	85 77	32,4 25,9	7,2	25,2 18,7	320 170	164,3±1,0 164,8±1,8	122±6 101±9	185±8 172±10
<sup>16</sup> O + <sup>204</sup> Pb	<sup>220</sup> Th	85 77	43,3 27,8	8,8	25,5 19,0		163,3±1,0 163,7±2,2		172±7 157±13
$^{16}O + ^{203}Tl$	<sup>219</sup> Ac	85	36,7	10,0	26,7		162,0±0,9	127±5	164±6

ion energy lies near the Coulomb barrier and the small one — by several MeV lower. Thus in the second case the fission cross section was 30—40 times smaller which determined the difference in the number of registered events  $(2-3)\times10^4$  for  $E_i=85$  MeV and  $(2-4)\times10^3$  for  $E_i=78$  MeV. Note also that at barrier energies  $(E_i < B_{fus})$  a compound nucleus is produced with  $\langle l^2 \rangle$  values typical for reactions with light charged particles which, at the above indicated energies  $E^*$ , occur higher the Coulomb barrier. This is of course a favourable circumstance for the comparative analysis of experimental data on low-energy fission.

Figures 1 and 2 present the results of measurements as complete mass distributions Y(M), symmetrized with respect to M = A/2 and normalized

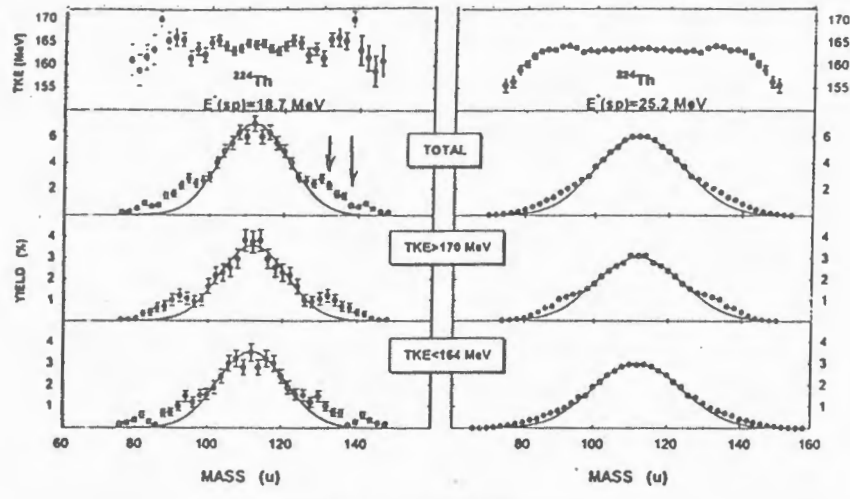
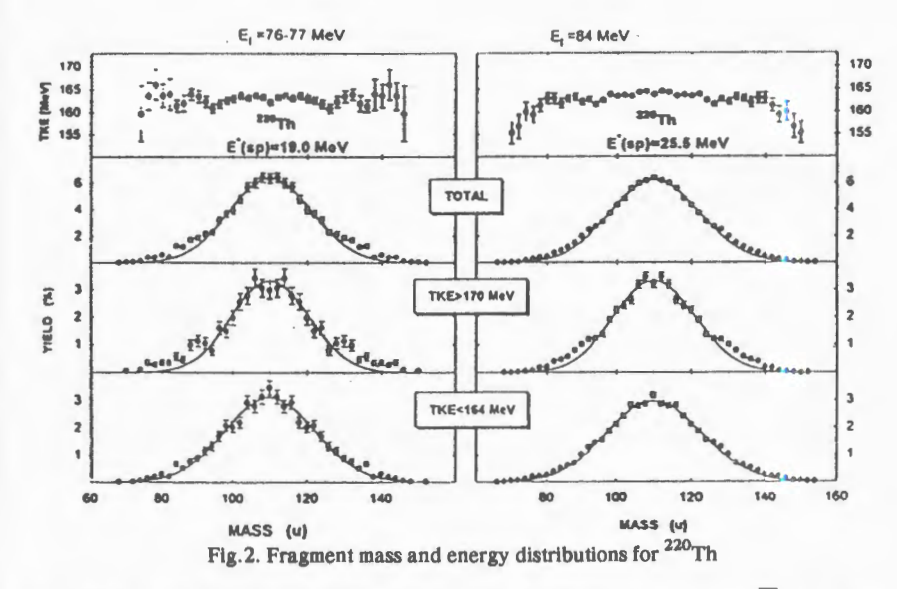


Fig. 1 Fragment mass and energy distributions for <sup>224</sup>Th



to 200%, and average kinetic energies of paired fragments  $\overline{E}_k(M)$  with masses M and A-M for  $^{224}$ Th and  $^{220}$ Th.

The curves in figs.1 and 2 present the results of the three-component analysis (according to the number of main fission modes, see above), presuming the Gaussian shape of partial distributions  $Y_i(M)$ . The indexes i denote: i = s — mass-symmetric fission mode with an average mass of fragment  $\overline{M} = A/2$ , i = a0 and a1 — mass-asymmetric fission modes with  $\overline{M}_{a0} = 139$  and  $\overline{M}_{a1} = 132$ , respectively.

Figure 3 presents exclusive yields of heavy fragments for the mass asymmetric nucleus of  $^{224}$ Th: the broken curves show the components  $Y_{a0}(M)$  and  $Y_{a1}(M)$  taken separately, the solid ones —the sum  $Y_a(M) = Y_{a0}(M) + Y_{a1}(M)$ , experimental points present the difference between the observed total yields and the curves describing the symmetric mode distribution. The yield of  $Y_a(M)$  increases noticeably with the cooling of the fissioning nucleus. The mass symmetric mode is dominating in the case of lighter nuclei. In full correspondence with subsequent outcome for the dependence of the  $Y_i(M)$  spectrum on the excitation energy and the nucleon content of fissioning nuclei, there changes the height of the  $\overline{E}_k(M)$  maximum in the part of figs.1,2, the apparition of which is explained by the

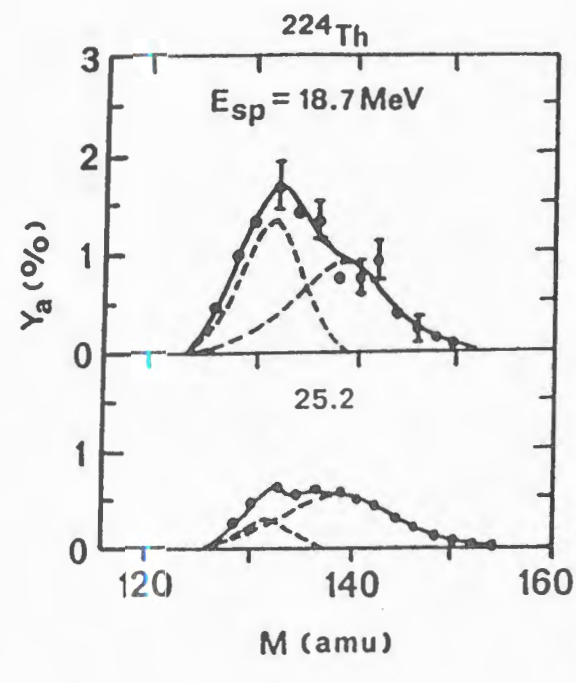


Fig.3. The yield of asymmetric modes  $Y_{a1}$  and  $Y_{a0}$  for  $^{224}$ Th

ratio for separate fission  $\overline{E}_k^s < \overline{E}_k^{a0} < \overline{E}_k^{a1}$ modes and that in accordance with this inequality at the discrimination of events with small fragment kinetic energies there takes place the enrichment of the mass distribution of fragments with asymmetric modes (at the fission of <sup>224</sup>Th it becomes trihumped) and, on the 160 contrary, at the discrimination of events with large fragment kinetic energies the mass

distribution gets free of them and becomes the same as in the symmetric mode.

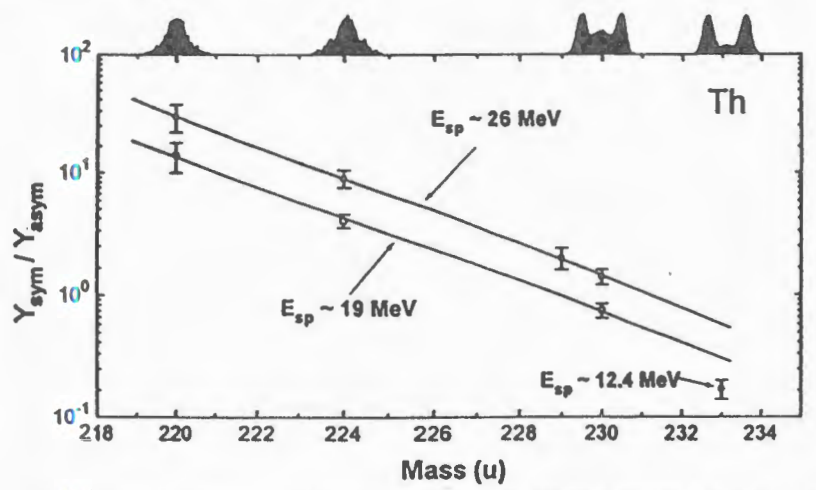


Fig. 4. The ratio symmetric and asymmetric components as function mass number A. The data for <sup>229</sup>Th, <sup>230</sup>Th, <sup>233</sup>Th from Refs. 10, 11, 12

The statistical accuracy of the performed measurements, especially for the lower and more interesting energy ( $E_{sp}^* \cong 19 \text{ MeV}$ ), is not sufficient for the deduction of numerous parameters, determining the yields  $Y_i(M)$  and the exact characteristics of separate modes, first of all the average energies of fragments  $\overline{E}_k^i$ .

Nevertheless, even at this initial stage of investigations a rather favourable situation for the discussion of two interesting observables has built up. The first one is dependence of  $Y_a^t/Y_s^t$  on the number of neutrons N in the chain of Th isotopes. It turns out that for the reactions  $^3\text{He} + ^{226}\text{Ra} \rightarrow ^{229}\text{Th}$  [10]  $^4\text{He} + ^{226}\text{Ra} \rightarrow ^{230}\text{Th}$  and [10,11] there are experimental data on the mass distributions of fission fragments at close excitation energies  $E_{sp}^*$ . The totality of data on the ratio  $Y_a^t/Y_s^t$  deduced from the results of [10,11] and of this work is presented in fig.4. The

significance of the scale of changes of Y(M), corresponding to the values of  $Y_a^t/Y_s^t$  is explicitly demonstrated by means of upper part of Fig.4 which the mass distributions themselves for a lower average energy  $E_{sn}^* \cong 19$  MeV. The picture becomes still more impressive in case the things shown in Fig.4 are extrapolated to A = 232-233. It follows from the experimental data on the fission of <sup>232</sup>Th by  $\gamma$ -quanta and neutrons [12] that in the corresponding to their mass distributions there will be observed a substantial domination of asymmetric component and they will have a dihumped shape which is traditional for the low energy fission of actinides.

The second most important factor determining the modal structure of the mass and energy distribution of the fragments is the experimental data about the kinetic energy spectrum of

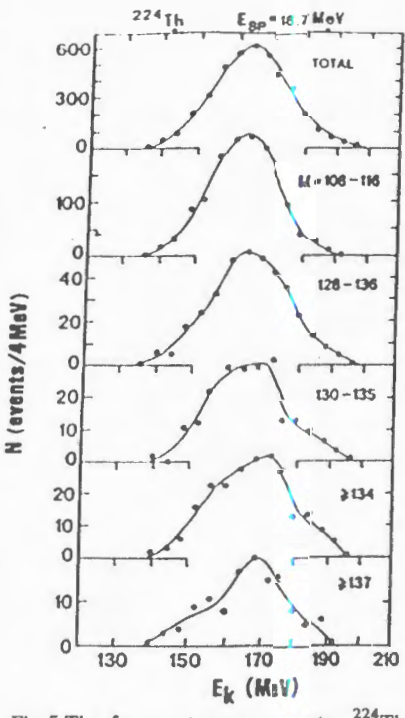


Fig.5.The fragment energy spectra <sup>224</sup>Th for different mass division

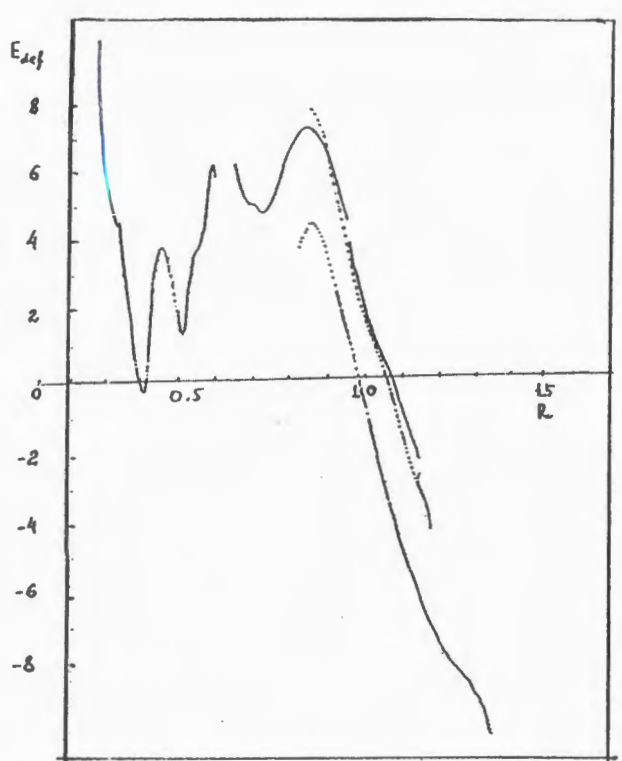
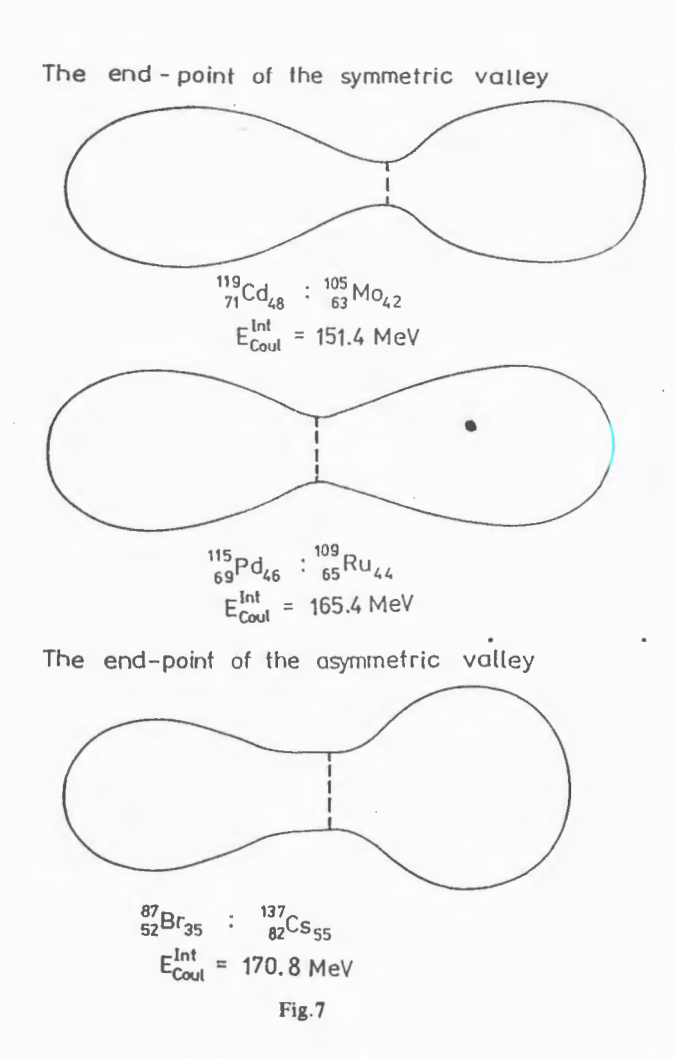


Fig.6. The calculations of deformation energy <sup>224</sup>Th as function of the distance between fragments

the fragments at different mass division, i.e.,  $M_N/M_L$ . The presence in such spectra of several precisely defined groups of fragments with different kinetic energies for specific  $M_T/M_L$  ratios (e.g., two groups in the Fm range and three groups in the Pb range) proves this new concept in fission physics. In our case we have also analysed the kinetic energy spectra of  $^{224}$ Th fission fragments having different mass, shown in Fig.5. The diagram demonstrates that despite the rather modest statistics we can observe in the  $E_k(M)$  spectrum all the main regularities occurring in the Pb-Fm range, i.e., three groups of fragments corresponding to the three different configurations of fissile nuclei at the scission point — one elongated (symmetrical fission) and two more compact configurations, determined by higher kinetic energy values of the fragments. This previous result certainly requires further investigation and more statistics.

In this respect, the work performed by us within the micro-macro approach [3] to the calculation of the deformation energy is of great interest and also predicts possible existence of 3 division modes of the <sup>224</sup>Th



nucleus. Figures 6 and 7 show the results of these calculations as a dependence of the deformation energy on the distance between the fragment centres during the process of the nucleus movement from the ground state to the scission point and as different configurations of the fissile nucleus at the moment of rapture corresponding to different fission modes. The obtained kinetic energy  $E_k^i$  values for different fission modes of  $^{224}$ Th on the whole correctly reflect the  $E_k^s < E_k^{a0} < E_k^{a1}$  ratio observed in the experiment.

#### Conclusion

Mass and energy distributions of low-energy fission fragment ( $E^* \cong 20-30$  MeV) in the reactions  $^{204,208}$ Pb and  $^{203}$ Te +  $^{16}$ O leading to the compound nuclei  $^{220}$ Th,  $^{224}$ Th and  $^{219}$ Ac are investigated.

As shown by the experiment, fragment mass and energy distributions for the studied nuclei have a clearly defined multimodal structure completely fitting the theoretical predictions given in the work for this nuclei range.

Analysis of the experimental results obtained in these measurements has led to the revelation of a new regularity, namely, the fact that the ratio of yields from the mass-symmetric and mass-asymmetric modes of fission changes by about two orders of magnitude in going from <sup>230</sup>Th to <sup>220</sup>Th. This result indicates that (by varying only the number of neutrons in a fissioning nucleus, say, in Th (or Ac, Ra, Fr) we can investigate all possible transformations of the fission fragment mass and energy distributions, from the mass-symmetric ones typical for nuclei lighter than lead, and the three-humped ones observed in the case of Ra, and Ac, to the traditional mass-asymmetric distributions which characterise the actinide region. In addition this makes it possible to establish a quantitative relationship between these transformations and the structural features of the potential energy of surfaces and the dynamics of collective motion.

One of us (V.V.Pashkevich) thanks IN2P3 for grant that made possible his stay in Bordeaux.

#### References

- Itkis M.G. et al. Z. Phys., 1985, A320, p.433; Nucl. Phys., 1989, A502, p.343.
- 2. Hulet E. et al. Phys. Rev., 1989, C40, p.770.
- Pashkevich V.V. Nucl. Phys., 1971, A169, p.175; Nucl. Phys., 1988, A477, p.1.
- 4. Oganessian Yu.Ts. Proc. of the Robert A. Welh Cong. on Chemical Research, Houston, Texas, 1990, p.159.
- 5. Murakami T. et al. Phys. Rev., 1986, C34, p.1353.
- 6. Rossner H. et al. Phys. Rev., 1992, C49, p.719.
- 7. Heinz A. et al. GSI-Report 93-1, 1993, p.364.
- 8. Chubarian G. et al. Yadernaya Fizika, 1993, 56.
- 9. Vandenbosch R. Ann. Rev. Nucl. Part., 1992, 42, p.447.
- 10. Britt H., Wegner H.E., Gursky J.L. Phys. Rev., 1963, 129, p.2239.

- Unik J.R., Huizenga J.R. Phys. Rev., 1964, 134, p.B90.
   Pleiffer E. Z.Phys., 1970, A250, p.50.

Received by Publishing Department on July 20, 1994.

# ИНКЛЮЗИВНЫЕ ЭНЕРГЕТИЧЕСКИЕ СПЕКТРЫ ЛЕГКИХ ЗАРЯЖЕННЫХ ЧАСТИЦ (p, d, t, $^4$ He) В СПОНТАННОМ ЛЕЛЕНИИ $^{248}$ Cm

И.В.Кузнецов, М.П.Иванов, В.Ф.Кушнирук, Ю.Г.Соболев, Г.В.Букланов

С помощью полупроводникового (dE-E)-телескопа измерены инклюзивные энергетические спектры частиц  $(p,d,t,^4\mathrm{He})$  в спонтанном делении  $^{248}\mathrm{Cm}$ . Наиболее вероятные энергии и ширины энергетических распределений, в пределах экспериментальных ошибок, совгадают с имеющейся совокупностью данных для широкого круга ядер, испытывающих низкоэнергетическое деление. Измеренная относительная вероятность эмиссии длиннопробежных  $\alpha$ -частиц согласуется с наблюдаемой зависиместью вероятности тройного спонтанного деления от параметра  $Z^2/A$  делящегося ядра для нуклидов с  $Z \ge 96$ . В спектре протонов наблюдается низкоэнергетическая компонента  $E_p \le 4$  МэВ, которая не может быть объясьма вкладом только от фоновых реакций (n,p) и  $(\alpha,p)$ .

Работа выполнена в Лаборатории ядерных реакций им.Г.Н.Флерова ОИЯИ.

The Inclusive Energy Spectra of Light Charged Particles (p, d, t, <sup>4</sup>He) from Spontaneous Fission of <sup>248</sup>Cm

#### I.V.Kuznetzov et al.

A semiconductor dE-E telescope was used to measure the inclusive energy spectra of light p, d, t,  $^4$ He particles from spontaneous fission of  $^{248}$ Cm. The most probable energies and the widths of the energy distributions of particles within the limits of experimental errors are consistent with available data for a wide range of nuclei undergoing low fission processes. The measured relative probability of the long range  $\alpha$ -particle emission is consistent with the observed dependence of the ternary spontaneous fission probability on the parameter  $Z^2/A$  of the fissioning nucleus for the nuclides with  $Z \ge 96$ . The proton energy spectra have at low-energy component with  $E_p \le 4$  MeV which cannot be explained as a contribution of the background (n, p) and  $(\alpha, p)$  reactions.

The investigation has been performed at the Flerov Laboratory of Nuclear Reactions, JINR.

Относительно редкие моды низкоэнергетического или спонтанного деления тягжелых ядер, в которых испускаются легкие заряженные частицы, являются предметом интенсивного экспериментального и теорс-

тического исследования с момента их открытия, поскольку представляют значительный интерес как для процесса деления, так и для теории ядерной материи в целом.

Сведения о результатах экспериментальных и теоретических исследований в этой области можно найти в обзорных работах [1—5].

К настоящему времени установлено, что энергетические спектры легких заряженных частиц (за исключением протонов) хорошо аппроксимируются гауссианами, наиболее вероятные энергии и щирины энергетических распределений частиц слабо зависят от параметра делимости  $Z^2/A$  в широком диапазоне зарядовых и массовых чисел Z и A делящихся ядер. С наибольшей вероятностью заряженные частицы вылетают почти перпендикулярно к оси разлета осколков деления. В экспериментах наблюдается повышенная вероятность (≅ 25%) тройного спонтанного деления по сравнению с тройным делением под действием нейтронов или у-квантов. Существующие теоретические модели испытывают трудности при попытках объяснить повышенную вероятность тройного спонтанного деления. В связи с этим представляет интерес расширение круга ядер, испытывающих тройное спонтанное деление, с целью изучения зависимости процесса эмиссии заряженных частиц от массы и заряда делящихся ядер. В данной работе впервые измерены инклюзивные энергетические спектры легких заряженных частиц  $(p, d, t, \alpha)$ , сопровождающих спонтанное деление <sup>248</sup>Cm, и относительная вероятность тройного спонтанного деления этого нуклида.

Идентификация и измерение энергии заряженных частиц проводились с помощью ( $\Delta E-E$ )-телескопа, состоящего из тонкого кремниевого поверхностно-барьерного  $\Delta E$ -детектора (30 или 500 мкм) и толстого (4 мм) Si (Li) E-детектора. Обогащенный источник  $^{248}$ Cm (96%) интенсивностью  $Y\cong 2\cdot 10^3$  дел./с., нанесенный на тонкую тигановую подложку, размещался на расстоянии 7 мм от телескопа, закрытого танталовой фольгой толщиной 19 мг/см², достаточной для поглощения  $\alpha$ -частиц естественного  $\alpha$ -распада изотопов Cm. Электронная система сбора информации представлена на рис.1а. Разрешение на запись события поступало от блока ВАП в случае совпадений логических сигналов временных отметок dE- и E-трактов в диапазоне 0,5 мкс.

Последующий «off-line» анализ производился при условии совпадений данных временных сигналов в интервале  $\Delta t \cong 30$  нс. Энергетические спектры частиц получались путем суммирования оцифрованных сигналов от dE- и E-детекторов в соответствующих областях: в двумерной «dE-E-матрице» (см. рис.16) с учетом энергетических потерь частиц в поглотительных фольгах.

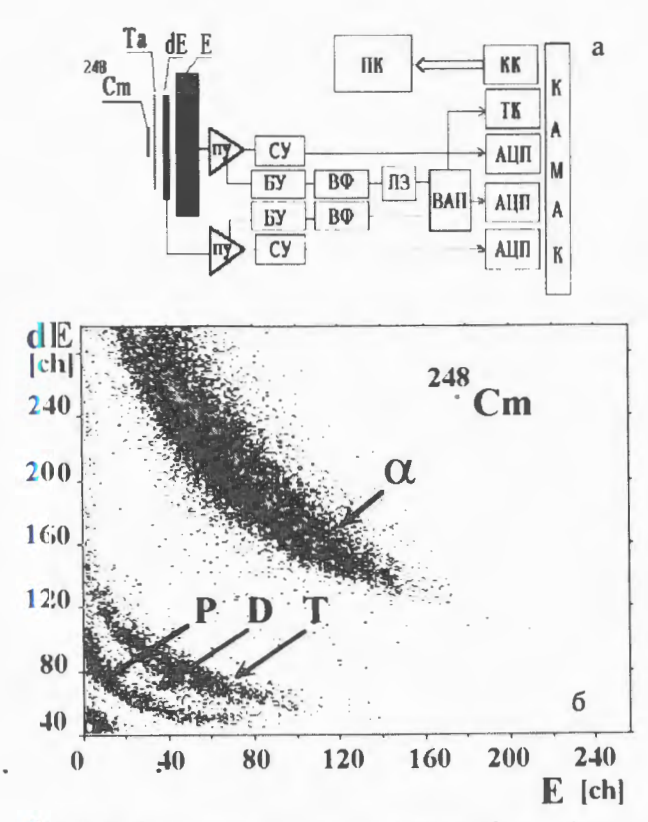
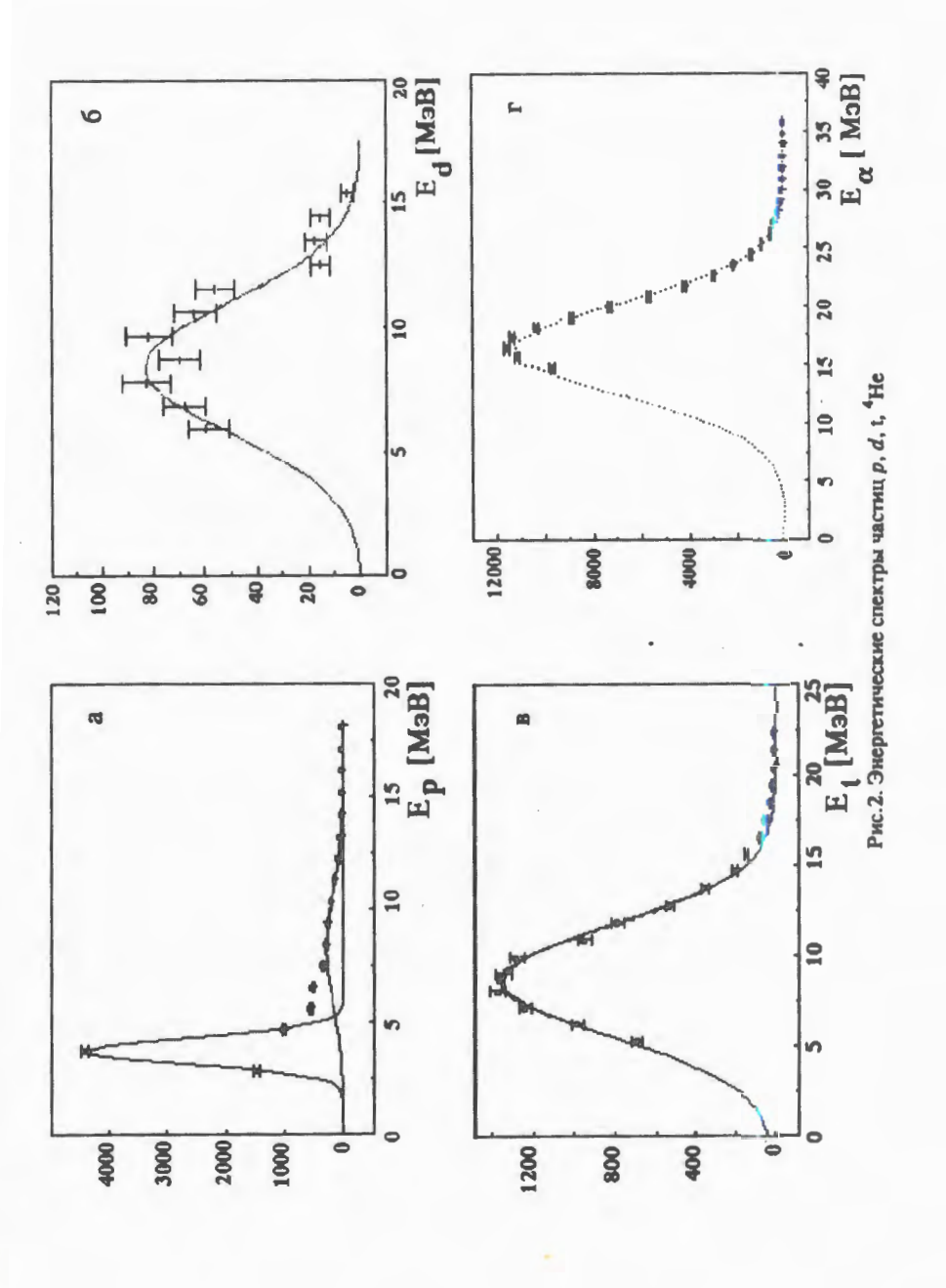


Рис.1. а) блок-схема электронной системы сбора информации, б) (dE-E)-матрица частиц p, d, t, <sup>4</sup>He

На рис. 2 приведены спектры частиц p, d, t, <sup>4</sup>He, измеренные в одной экспозиции. Гладкой кривой приведены результаты  $\chi^2$ -аппроксимации спектров гау ссианами. Из рис. 2 видно, что экспериментальные спектры d-, t-, <sup>4</sup>He-частиц хорошо описываются распределением Гаусса, а спектр протонов имеет сложную структуру. Подобная форма спектра протонов наблюдалась также в спонтанном делении <sup>252</sup>Cf [6,7]. Низкоэнергетическая компонента спектра протонов в указанных работах была отнесена к фонсвым (n,p)- и  $(\alpha,p)$ -реакциям на примесях материала поглотителей, исгочника и детекторов. Однако в работе [8] выход низкоэнергетических прютонов в спонтанном делении <sup>252</sup>Cf авторы не смогли объяснить за счет фоновых реакций. Энергетический спектр протонов в области энергий  $E_p \ge 4$  МэВ нами, так же, как и авторами работ [6,7],



фитировался гауссианом и был отнесен к протонам, связанными с тройным делением.

В таблице приведены полученные из измеренных спектров наиболее вероятные энергии, ширины энергетических распределений и относительные экстраполированные выходы легких заряженых частиц в сравнении с известными характеристиками частиц, сопровождающих спонтанное деление <sup>252</sup>Cf. Из таблицы видно, что параметры, описывающие энергетические характеристики частиц для деления 248Ст и <sup>252</sup>Сf. в пределах экспериментальных ошибок, совпадают. На основании этого наблюдения можно предположить, что тройное спонтанное деление <sup>248</sup>Ст характеризуется теми же закономерностями, которые присущи тройному спонтанному делению <sup>252</sup>Cf и другим ядрам, испытывающим низкоэнергетическое тройное деление. Для измерения относительной вероятности эмиссии <sup>4</sup>Не в тройном делении <sup>248</sup>Сm и <sup>252</sup>Сf сначала измерялся выход осколков деления с помощью dE-детектора телескопа, а затем, после установки танталовой фольги, выход  $\alpha$ -частиц. Отношение выхода <sup>4</sup>Не к двойному делению, усредненное по нескольким измерениям, составило  $2,0\pm0,3$  и  $3,0\pm0,3$  для  $^{248}{\rm Cm}$  и  $^{252}{\rm Cf}$ соответственно. На рис. 3 приведены результаты наших измерений (от-

Таблица. Параметры энергетических спектров и выходы легких ядер

Частица	Измер.диапазон энергии, МэВ	Наиболее веро- ятн. энергия, МэВ	пшпм, мэв	Экстрапол. вы- ход на 10 <sup>4 4</sup> Не	Лит
		<sup>248</sup> Cm			
<sup>1</sup> H	8,5-18,2	8,3±0,5	5,7±0,5	160±20	*)
<sup>2</sup> H	6,2:—15,5	8,4±0,5	6,2±0,6	50±5	*)
<sup>3</sup> H	5,2-22,5	8,7±0,3	8,0±0,2	922±18	*)
<sup>4</sup> He	14,8-36,0	16,4±0,2	9,5±0,3	104	*)
	•)	— результаты насто	оящей работы		
		<sup>252</sup> Cf			
<sup>1</sup> H	7,3-18,8	7,8±0,8	6,8±0,8	175±30	[6]
<sup>2</sup> H	5,3-21,5	8,0±0,5	7,2±0,7	68±3	[8]
<sup>3</sup> H	4,0-20,0	8,3±0,1	7,0±0,1	836±12	[10]
<sup>4</sup> He	8,3-37,3	16,0±0,2	9,9±0,7	10 <sup>4</sup>	[6]
<sup>4</sup> He	8.0-28.0	15,8±0,1	10,2±0,1	104	[10]

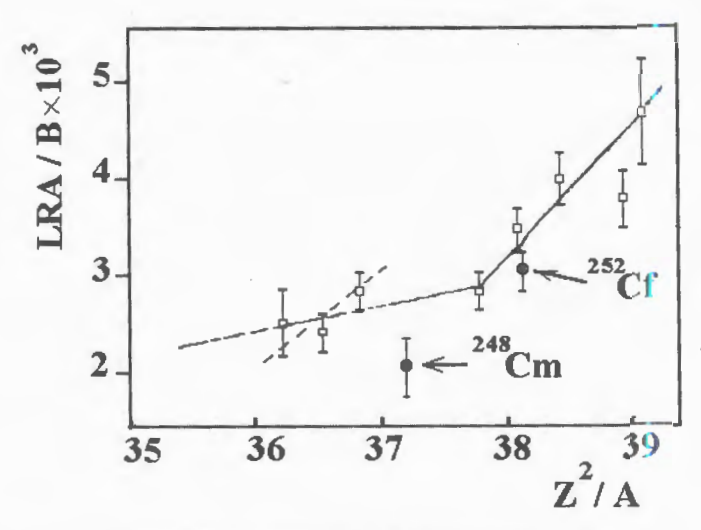


Рис.3. Вероятность эмиссии  $^4$ Не в зависимости от  $Z^2/A$ 

меченные заполненными кружками) совместно с известными [9] данными по зависимости относительной вероятности эмиссии  $\alpha$ -частиц от величины параметра  $Z^2/A$  делящегося ядра. Сравнение данных настоящей работы с литературными показывает, что крутой спад относительной вероятности тройного спонтанного деления сохраняется вплоть до величины параметра делимости  $Z^2/A \cong 37$ .

Для выяснения природы низкоэнергетической части протонного спектра были проведены дополнительные опыты:

Влияние (n,p)-реакций, вызываемых нейтронами делєния в танталовой фольге и материале детекторов, исследовалось в эксперименте, в котором между источником  $^{248}\mathrm{Cm}$  и телескопом помещался танталовый поглотитель толщиной  $\cong 1300~\mathrm{mr/cm}^2$ , останавливающий протоны с энергией  $E_p \le 25~\mathrm{M}{}$  ЭВ и  $\alpha$ -частицы с  $E_\alpha \le 90~\mathrm{M}{}$  ЭВ. В результате измерения было установлено, что верхняя граница вклада в низкоэнергетическую часть спектра протонов от (n,p)-реакций, вызываємых нейтронами деления, составила не более 10%.

С целью выяснения вклада протонов отдачи от  $\alpha$ -части и осколков деления, непосредственно между источником  $^{248}$ Cm и поглотительной фольгой (19 мг/см²) помещалась майларовая фольга, ссідержащая  $\cong 10^{18}$  см $^{-2}$  атомов водорода. В результате измерения было установлено, что вклад протонов отдачи от упругого рассеяния  $\alpha$ -частиц и оскол-

ков деления на водородосодержащих примесях в мишени и танталовой фольге принебрежимо мал.

Таким образом, дополнительные опыты показали, что выход низкоэнергетических протонов невозможно объяснить только за счет фоновых реакций.

Для дальнейшего исследования механизма эмиссии низкоэнергетических протонов в спонтанном делении целесообразно провести эксперименты с более низким энергетическим порогом регистрации протонов в совпадении с осколками деления.

Авторы благодарны Ю.Э.Пенионжкевичу за постоянную поддержку при проведении настоящей работы, Б.И.Пустыльнику и Ю.В.Пяткову за полезные обсуждения, Э.М.Козулину и Ю.В.Лобанову за помощь в работе.

### Литература

- 1. Перфилов Н.А. Романов Н.Ф., Соловьев Э.И. УФН, 1961, т.71, № 3, с.200.
- 2. Hyde E.K., In: The Nuclear Properties of Heavy Elements, vol.III, Prentice-Hall, Englewood Cliffs. N.G., 1964, p.131.
- 3. Halpern I. Ann. Rev. Nucl. Sci., 1971, vol.21, p.245.
- 4. Гусев Ю.И., Селиверстов Д.М. Материалы 25 Зимней школы ЛИЯФ 1990, Л.: ЛИЯФ, 1990, с.35.
- 5. Theobald J. In: School-Seminar on Heavy Ion Physics, JINR, 7-93-274, Dubna, vol.1, p.262.
- 6. Cosper S.W., Cerny J., Gatti R.S. Phys. Rev., 1967, vol. 154, p.1193.
- 7. Gavron A., Gazit Y. Phys. Rev., 1974, vol.10, No.1, p.388.
- Budzanovski A., Karcz W., Siwek A., Skwiczynska I., Wolski R. Raport IFI N1509/PL, Krakow, 1990.
- Wagemans C. In: Proc. Int. Workshop on Dynamical Aspects of Nuclear Fission, JINR, E7-52-95, Dubna, 1992, p.139.
- Грачев В.Т., Гусев Ю.И., Селиверстов Д.М. ЯФ, 1988, т.47, вып.3, с.627.

## NUCLEON CORRELATION EFFECTS ON Y-SCALING QUANTITIES IN NUCLEI\*

M.K.Gaidarov<sup>1</sup>, A.N.Antonov<sup>1</sup>, S.S.Dimitrova<sup>1</sup>, M.V.Stoitsov<sup>1</sup>

The asymptotic scaling function F(y) and the binding correction B(y) as well as the mean kinetic and removal energies are calculated in the cases of the <sup>4</sup>He, <sup>12</sup>C, <sup>16</sup>O and <sup>40</sup>Ca nuclei using the nucleon momentum distributions obtained within the Jastrow correlation method and the phenomenological model accounted for short-range and tensor nucleon-nucleon correlations. The scaling functions F(y) differ from those obtained in the mean-field approximation and are in qualitative agreement with the available experimental data. It is shown that the binding correction B(y) can be explicitly evaluated using a realistic nuclear spectral function. The account for the nucleon-nucleon correlations gives increased values of the mean kinetic  $\langle T \rangle$  and mean removal  $\langle E \rangle$  energy (in comparison with their values in the mean-field approximation) and leads to correct values of the binding energy per nucleon in the nuclei considered.

The investigation, has been performed at INRNE (Bulgaria) in collaboration with LTP, JINR.

# Нуклонные корреляционные эффекты на У-скейлинговых величинах в ядрах

М.К.Гайдаров, А.Н.Антонов, С.С.Димитрова, М.В.Стоицов

Асимптотическая скейлинговая функция F(y), поправка на энергию связи B(y), а также средние кинетическая и энергия связи вычислены для ядер  ${}^4\text{He}$ ,  ${}^{12}\text{C}$ ,  ${}^{16}\text{O}$  и  ${}^{40}\text{Ca}$  с использованием нуклонных импульсных распределений, полученных в рамках метода ястровских корреляций и феноменологической модели, учитывающей короткодействующие и тензорные нуклон-нуклонные корреляции. Скейлинговые функции F(y) отличаются от полученных в приближении среднего поля и находятся в качественном согласии с имеющимися экспериментальными данными. Показано, что поправка на связь B(y) точно оценена с использованием реалистичной ядерной спектральной функции. Учет нуклон-нуклонных корреляций дает увеличенные значения средней кинетической энергии  $\langle T \rangle$  и средней энергии связи  $\langle E \rangle$  по сравнению с их значениями в приближении среднего поля и ведут к правильным значениям энергии связи на нуклон для рассмотренных ядер.

Работа выполнена в ИЯИЯЭ (Болгария) в сотрудничестве с ЛТФ,

<sup>\*</sup>This work is partially supported by the Bulgarian National Science Foundation under the Contract No.Φ-32.

<sup>&</sup>lt;sup>1</sup>Permanent address: Institute of Nuclear Research and Nuclear Energy, Bulgarian Academy of Sciences, Sofia 1784, Bulgaria.

#### 1. Introduction

Significant part of the recent nuclear experiments, both in high and low energies, poses the question about the limits of the mean-field approximation (MFA) in nuclear theory. We shall mention the deep-inelastic proton, inclusive and exclusive electron-scattering in nuclei which show the existence of high-momentum components in the nucleon momentum distribution as well as partial depletion of the levels below the Fermi level and partial filling above it in the nuclear ground state [1]. These results are in contradiction with the predictions of the shell model. The reason of this are the effects of short-range and tensor nucleon-nucleon correlations in nuclei which are related to specific peculiarities of the nucleon-nucleon forces at small distances. This imposes the development of correlated methods in nuclear theory which are going beyond the limits of the MFA.

A plausible method for studying of short-range correlation (SRC) effects in nuclei is the y-scaling method [2-10]. Since West's pioneer work [2], there has been a growth of interest in y-scaling analysis, both in its experimental and theoretical aspects. This is motivated by the importance of extracting nucleon momentum distributions from the experimental data. Furthemore, the y-scaling method enables us to see how the characteristics of the system considered at finite momentum transfer q differ from those obtained in the framework of the Plane Wave Impulse Approximation (PWIA). From experimental point of view, the possibility of extracting the nucleon momentum distribution from the inclusive electron quasielastic scattering data relies on the knowledge of the scaling function in the asymptotic limit and there are no clear criteria to decide whether the available data which are necessarily obtained for large but finite values of q can be associated with those from the analysis of the true asymptotic region. It has been shown that if a proper theory of y-scaling (taking into account the nucleon binding and momentum) is adopted, then the extracted nucleon momentum distributions are in good agreement with those obtained in a more direct way from the exclusive electron scattering (e, e'p) experiments. This fact confirms the expectation that the corresponding asymptotic scaling function should agree with the experimental one even if the experimental data are affected by the final state interaction (FSI).

A detailed study of the momentum distribution and its relation with the spectral function shows that it can be divided into two parts corresponding to low- and high-momentum components. These components in the nucleus with A nucleons are associated with the ground state and high virtual excitations of the spectator system with A-1 nucleons. Such investigation allows one to calculate the scaling function and some important nuclear characteristics.

In this paper we connect the results on the SRC effects obtained in the Jastrow correlation method (JCM) [11-13] and in the phenomenological method (PM) accounting for short-range and tensor correlations from 114,15 I with the quantities which are analysed in the y-scaling method. The aim of our work is, using the nucleon momentum distributions obtained in the correlation methods mentioned above, to calculate the scaling function, the binding correction function as well as the mean kinetic and mean removal energies in <sup>4</sup>He, <sup>12</sup>C, <sup>16</sup>O and <sup>40</sup>Ca nuclei. The results for the asymptotic function are compared with the available experimental data for the cases of <sup>4</sup>He and <sup>12</sup>C nuclei. This comparison serves as a test for the correlation methods. The results for the 160 and 40 Ca nuclei are predictions of the JCM and PM concerning the y-scaling quantities. The calculations of the binding correction function and the mean kinetic and removal energies give an additional information on the extent to which the SRC are accounted for in the correlation methods considered in the present work and on their reliability analyzing quantities which are sensitive to the SRC.

The definitions and discussion of the main y-scaling quantities, as well as the basic relationships of the correlation methods considered in this work are given in Section 2 of the paper. The results for the asymptotic scaling function, for the binding correction function, as well as for the mean kinetic and mean removal energies are presented in Section 3. The concluding remarks are given in Section 4.

### 2. Theoretical Basis

### 2.1. The Y-Scaling Method

The general concepts of the y-scaling method for the description of the electron quasielastic scattering by nuclei have been introduced by West [2]. Using the scaling variable y as a kinematical variable, the inclusive cross section  $\sigma_2$  can be presented in the PWIA in the form [10]:

$$\sigma_2 = (Z\overline{\sigma_{\rm ep}} + N\overline{\sigma_{\rm en}}) \left| \frac{\partial \omega}{k\partial \cos \alpha} \right|^{-1} F(q, y),$$
 (1)

where  $\overline{\sigma_{\text{ep}(n)}}$  is the relativistic electron-proton (neutron) cross section in the scattering of an electron by an off-shell nucleon with momentum k,  $\omega(q)$  is

the energy transfer, q is the momentum transfer and  $\left| \frac{\partial \omega}{k \partial \cos \alpha} \right|^{-1}$  is the

kinematical factor. The nuclear structure function

$$F(q, y) = 2\pi \int_{E_{\min}}^{E_{\max}(q, y)} dE \int_{k_{\min}(q, y, E)}^{k_{\max}(q, y, E)} P(k, E) k dk$$
 (2)

is a function of q and the scaling variable

$$y = (kq)/q = M(\omega - q^2/2M)/q.$$
 (3)

In (2) P(k, E) is the spectral function, the limits of integration are determined by the energy conservation,  $E_{\min} = |E_A| - |E_{A-1}|$ ,  $E_A$  and  $E_{A-1}$  being the ground state energies of the A and A-1 nuclei, respectively. The scaling variable y satisfies the equation:

$$\omega + M_A = [M^2 + (q + y)^2]^{1/2} + [M_{A-1}^2 + y^2]^{1/2}, \tag{4}$$

where  $M_A$  and  $M_{A-1}$  are the masses of the A and A-1 nuclei in their ground state. y has a meaning of a minimal longitudinal (along q) momentum of a nucleon with the minimal value ( $E_{\min} = M + M_{A+1} - M_A$ , M being the proton mass) of the separation energy, i.e.,  $|y| = k_{\min}(E_{\min})$ . The spectral function in (2) is usually given in the general form:

$$P(k, E) = P_{gr}(k, E) + P_{ex}(k, E),$$
 (5)

where

$$P_{gr}(k, E) = n_{gr}(k) \delta (E - E_{min})$$
 (6)

is the probability distribution that the final (A-1) system is left in the ground state (corresponding to the excitation energy  $E_{A-1}^*=0$  and  $E=E_{\min}$ ), whereas  $P_{\rm ex}(k,E)$  is probability distribution that the final (A-1) system is left in any of its excited states (with  $E_{A-1}^*\neq 0$ ,  $E=E_{\min}+E_{A-1}^*$ ). The relation between the spectral function and the momentum distribution is

$$n(k) = \int_{E_{\min}}^{\infty} P(k, E) dE = n_{\rm gr}(k) + \int_{E_{\min}}^{\infty} P_{\rm ex}(k, E) dE = n_{\rm gr}(k) + n_{\rm ex}(k).$$
 (7)

Indeed, the momentum distribution can be presented as follows:

$$n(\mathbf{k}) = |\langle \Psi_0^{(A-1)} | \hat{\Psi}(\mathbf{k}) | \Psi_0^{(A)} \rangle|^2 + \sum_{f \neq 0} |\langle \Psi_f^{(A-1)} | \hat{\Psi}(\mathbf{k}) | \Psi_0^{(A)} \rangle|^2,$$
 (8)

where  $\widehat{\Psi}(\mathbf{k})$  is the annihilation operator of a nucleon with momentum  $\mathbf{k}$ ,  $\Psi_0^{(A)}$  is the wave function of the ground state of the A-nucleon system,  $\Psi_0^{(A-1)}$  and  $\Psi_f^{(A-1)}$  are the wave functions of the (A-1)-nucleon system in its ground and excited (f) state, respectively. It can be seen that the first term in (8) reproduces  $n_{\rm gr}(k)$ , whereas the second one gives  $n_{\rm ex}(k)$  from (7).

The separation of the spectral function (5) has been adopted (e.g., [6,10]) in order to single out the nucleon binding effect (coming from  $P_{\rm ex}(k,E)$ ) on the scaling function. We use model spectral functions in which only average excitation energy of the final nuclear system is considered:

$$P_{\rm ex}(k,E) = n_{\rm ex}(k) \,\delta \, (E - \overline{E_{\rm ex}}). \tag{9}$$

The value of  $\overline{E_{\rm ex}}$  can be calculated from the energy weighed sum rule [16]:

$$\frac{E_A}{A} \equiv |\epsilon_A| = \frac{1}{2} \left\{ \langle E \rangle - \langle T \rangle (A - 2) / (A - 1) \right\},\tag{10}$$

where

$$\langle T \rangle = \int (k^2/2M) P(k, E) dk dE$$
 (11)

and

$$\langle E \rangle = \int EP(k, E) dk dE$$
 (12)

are the mean kinetic and mean removal energies, respectively, and  $|\epsilon_A|$  is the binding energy per particle. It follows from (5), (6), (9) and (12) that

$$\langle E \rangle = E_{\min} S_{gr} + \overline{E_{ex}} S_{ex},$$
 (13)

where

$$S_{\rm gr} = 4\pi \int n_{\rm gr}(k) k^2 dk \tag{14}$$

and

$$S_{\rm ex} = 4\pi \int n_{\rm ex}(k) k^2 dk \tag{15}$$

are the occupation probabilities. The normalization of the spectral function is

$$4\pi \int P(k, E) k^2 dk dE = 1. \tag{16}$$

It was shown in [8] that due to the behaviour of the spectral function P(k, E) at large k and E and using eq. (5), the structure function can be presented in the form:

$$F(q, y) = 2\pi \int_{|y|}^{\infty} n_{gr}(k) k dk + 2\pi \int_{E_{min}}^{\infty} dE \int_{k_{min}(q, y, E)}^{\infty} P_{ex}(k, E) k dk,$$
 (17)

where the first term scales in y, but the second term represents a «scaling violation»  $(k_{\min}$  depends on q) due to the nucleon binding. In the asymptotic limit  $(q \to \infty)$ 

$$\lim_{q \to \infty} k_{\min}(q, y, E) \equiv k_{\min}^{\infty}(y, E) \cong |y - (E - E_{\min})|$$
 (18)

one has:

$$F(y) = 2\pi \int_{|y|}^{\infty} n_{gr}(k) k dk + 2\pi \int_{E_{min}}^{\infty} dE \int_{|y-(E-E_{min})|}^{\infty} P_{ex}(k, E) k dk,$$
 (19)

OF

$$F(y) = f(y) - B(y), \tag{20}$$

where

$$f(y) = 2\pi \int_{|y|}^{\infty} n(k) k dk$$
 (21)

is the longitudinal momentum distribution and

$$B(y) = 2\pi \int_{E_{-1}}^{\infty} dE \int_{|y|}^{|y-(E-E_{\min})|} P_{ex}(k, E) k dk$$
 (22)

is the contribution arising from  $P_{ex}(k, E)$  representing the binding correction to the scaling function.

After taking the derivative of both sides of (20) one gets for the nucleon momentum distribution (NMD):

$$n(k) = -\frac{1}{2\pi y} \left[ \frac{dF(y)}{dy} + \frac{dB}{dy} \right], \qquad k = |y|. \tag{23}$$

Hence, the extraction of the NMD in the y-scaling approach needs the asymptotic scaling function F(y) to be obtained from the experimental data and the binding correction to the NMD dB/dy to be obtained in a realistic way.

The experimental inclusive cross sections  $\sigma_2$  for <sup>3</sup>He [17,18], <sup>4</sup>He, <sup>12</sup>C and <sup>56</sup>Fe [19] and for the nuclear matter [20] give the possibility of determining the experimental scaling function [7,8]:

$$F_1^{\exp}(q, y) = \frac{\sigma_2^{\exp}(q, \omega)}{(Z\sigma_{\rm ep} + N\sigma_{\rm en})} \left[ \frac{d\omega}{k\partial \cos \alpha} \right]. \tag{24}$$

The experimental knowledge of the asymptotic scaling function F(y) and the estimate of the binding corrections B(y) for <sup>3</sup>He and for complex nuclei [21,22] allow the NMD for <sup>2</sup>H, <sup>3</sup>He, <sup>4</sup>He, <sup>12</sup>C, <sup>56</sup>Fe and nuclear matter to be obtained [8] using (23). The results for various nuclei confirmed the conclusion that n(k) at  $k \le 1$  fm<sup>-1</sup> can be predicted by the mean field methods, but for  $k \ge 2$  fm<sup>-1</sup> the NMD behaviour depends on correlation effects in nuclei and is almost independent of the mass number A.

In this work we shall apply the NMD obtained in JCM and in the PM accounted for SRC and tensor correlations to calculate the scaling function F(y) and to compare directly with the available experimental data for F(y) in <sup>4</sup>He and <sup>12</sup>C as well as the binding correction to the scaling function B(y) and the mean kinetic and removal energies in the cases of <sup>4</sup>He, <sup>12</sup>C, <sup>16</sup>O and <sup>40</sup>Ca nuclei. The basic relations of the correlation methods used in the calculations are given in the next subsection.

## 2.2. Phenomenological Correlation Methods

A method to account for the short-range repulsion in the nucleon-nucleon force has been developed by Jastrow [23]. In it the total many-body wave function is written in the form

$$\Psi(\mathbf{r}_{1},...,\mathbf{r}_{A}) = C_{A}^{-1/2} \prod_{1 \le i \le j \le A} f(\mathbf{r}_{ij}) \Phi(\mathbf{r}_{1},...,\mathbf{r}_{A}), \tag{25}$$

where A is the number of nucleons with particle coordinates  $\mathbf{r}_1$ ,  $\mathbf{r}_2$ ,...,  $\mathbf{r}_A$ ,  $\Phi$  is a Slater determinant built up from single-particle wave functions  $\varphi_\alpha(\mathbf{r})$  which correspond to the occupied states, and  $C_A$  is the normalization constant. The correlation function  $f(\mathbf{r}_{ij}) = f(|\mathbf{r}_i - \mathbf{r}_j|)$  satisfies the conditions:

$$f(r_{ij}) = 0, \quad \text{for } |\mathbf{r}_i - \mathbf{r}_j| \le r_c,$$
  

$$f(r_{ij}) = 1, \quad \text{for } |\mathbf{r}_i - \mathbf{r}_j| \to \infty,$$
(26)

where  $r_c$  is the radius of the nucleon-nucleon repulsive core. The wave function  $\Psi$  [eq. (25)] is used as a trial function in varitional calculations of the energy for a system with a given Hamiltonian. Various approximations and appropriate techniques which are based on the variations with respect to the single-particle functions  $\varphi_{\alpha}(\mathbf{r})$  and the correlation function  $f(r_{ij})$  have been developed in the JCM.

Gaudin et al. [24] suggested a perturbation expansion method for calculating the one- and two-body density martices. These quantities are written as an expansion in terms of the functions

$$g(r) = |f(r)|^2 - 1, h(r) = f(r) - 1.$$
 (27)

Using the lowest-order-cluster approximation, harmonic-oscillator single-particle wave functions and Gaussian form for the function f(r), the nucleon momentum distribution n(k) for <sup>4</sup>He has been obtained [11] and compared with the exact Jastrow calculations [25]. An important feature of n(k) is the high-momentum tail at k > 2 fm<sup>-1</sup>. This result shows the role of the Jastrow-type SRC on the high-momentum components of the momentum distribution.

In [12,13] the JCM in its lowest-order approximation (LOA) is applied to calculate short-range correlation effects on the nucleon momentum and density distributions, as well as on the occupation probabilities and natural orbitals in the <sup>4</sup>He, <sup>16</sup>O and <sup>40</sup>Ca nuclei. The obtained analytical expressions for the one-body density matrix, for the momentum and density distributions in [12,13] give a possibility for a detailed study of the quantities sensitive to the SRC.

The short range and tensor correlation effects on the nucleon momentum distributions and form factor have been studied within the phenomenological model from [14,15]. The two-body correlation operator u(1, 2) acting on the pair wave function is introduced in the two-body density matrix of the correlated system:

$$\rho(v_{1}, v_{2}; v_{1}^{'}, v_{2}^{'}) = \sum_{a, b} [\langle v_{1}v_{2} | u(1, 2) | ab \rangle \langle ab | u^{+}(1, 2) | v_{1}^{'}v_{2}^{'} \rangle - \langle v_{1}v_{2} | u(1, 2) | ab \rangle \langle ab | u^{+}(1, 2) | v_{2}^{'}v_{1}^{'} \rangle],$$
(28)

where  $v = (\mathbf{r}_i, s_i^z, t_i^z)$ . In the case of the harmonic-oscillator single-particle wave functions the two-particle state function  $|a(1), b(2)\rangle$  is expanded on the basis of the relative and c.m. coordinates, the total angular momentum, and spin and isospin of the pair:

$$|a(1), b(2)\rangle = \sum_{ab} |nlm\rangle |NLM\rangle |SS^2\rangle |TT^2\rangle,$$
 (29)

where N, L, M; n, l, m are the radial and angular c.m. and relative motion quantum numbers; S, T, the spin and isospin of the pair; and  $S^z$  and  $T^z$ , their third components.

The SRC effects are included by means of the operator  $u(1, 2)_{s.r.}$  acting on the radial part of the pair wave function

$$[u(1,2)]_{s,r} | nlm \rangle = N_{nl}^{-1/2} f(r) | (nlm) \rangle, \tag{30}$$

with

$$f(r) \xrightarrow{r \to 0} 0, \qquad f(r) \xrightarrow{r \to \infty} 1.$$
 (31)

The tensor correlations are included by using the two-body operator  $u(1, 2)_{tens}$  that acts both on the angular and the radial parts of the relative motion of the pair. In practical applications the tensor operator is restricted to deuteron-like states only:

$$[u(1,2)]_{\text{tens.}} |n^3, S_1, J^z, T = 0\rangle = (1 - \eta^2)^{1/2} \varphi_{n0}(r) |n, {}^3S_1, J^z, T = 0\rangle + \eta \varphi_{n2}(r) |n, {}^3D_1, J^z, T = 0\rangle,$$
(32)

where  $\varphi_{nl}(r)$  are the radial wave functions, chosen to be the harmonic-oscillator fuctions.

Explicit expressions for the nucleon momentum distributions and form factors are obtained for the  $^4$ He,  $^{16}$ O and  $^{40}$ Ca nuclei in [15]. It is shown that the effects of both short-range and tensor correlations lead to the existence of the high-momentum tail of the momentum distribution n(k) which is several orders of magnitude higher than the values of n(k) in the independent-particle models. The tensor correlations are stronger for light nuclei ( $^4$ He and  $^{16}$ O) than for  $^{40}$ Ca.

The detailed study of the NMD in the JCM [12,13] and in the PM from [14,15] shows that it can be separated into two terms,  $n(k) = n_1(k) + n_2(k)$ , where the first one  $(n_1(k))$  corresponds to the low-momentum region  $(k < 2 \text{ fm}^{-1})$ ; and the second one  $(n_2(k))$ , to the high-momentum region  $(k \ge 2 \text{ fm}^{-1})$ . This can be related to the conclusion from [8] that the NMD at  $k \ge 2 \text{ fm}^{-1}$  is entirely exhausted by  $n_{ex}(k)$ . The latter allows us to identify  $n_{gr}(k)$  and  $n_{ex}(k)$  from (7) with  $n_1(k)$  and  $n_2(k)$ , respectively, and to calculate the scaling function, the binding correction to it and the mean kinetic and removal energies within the JCM and the PM for various nuclei.

#### 3. Results of Calculations and Discussion

## 3.1. Scaling Function and Binding Correction

The effects of the nucleon correlations accounted in the JCM [12,13] and in the PM [14,15] on the y-scaling function F(y) and the binding correction B(y) can be calculated using the momentum distributions obtained in both correlation methods in eqs. (19-22) and the model spectral functions (eqs. (5,6,9)). The theoretical results for the functions F(y) and B(y) in the <sup>4</sup>He, <sup>12</sup>C, <sup>16</sup>O and <sup>40</sup>Ca nuclei obtained by using the nucleon momentum distributions from the JCM method [12,13,26] are given in Figs.1-4. We note that: i) At low values of |y| ( $|y| \le 350 \text{ MeV/c}$ ) the shape of F(y) for a given nucleus is determined mainly by the first term of eq. (19), which scales in y and is generated by  $n_{gr}(k)$ . The latter is similar to the momentum distribution predicted in the mean-field approximation; ii) At higher values of |y| (|y| > 350 MeV/c) the function F(y) is almost entirely determined by the second term of eq. (19), which is generated by  $n_{ex}(k)$ , i.e. by the highmomentum part of the momentum distribution. The function  $n_{ex}(k)$  is almost independent of the mass number A and contains the effects of the SRC. Concerning the binding correction B(y) to the scaling function we note that it is almost constant at  $y \le -100 \text{ MeV/c}$  and is quite appreciable at

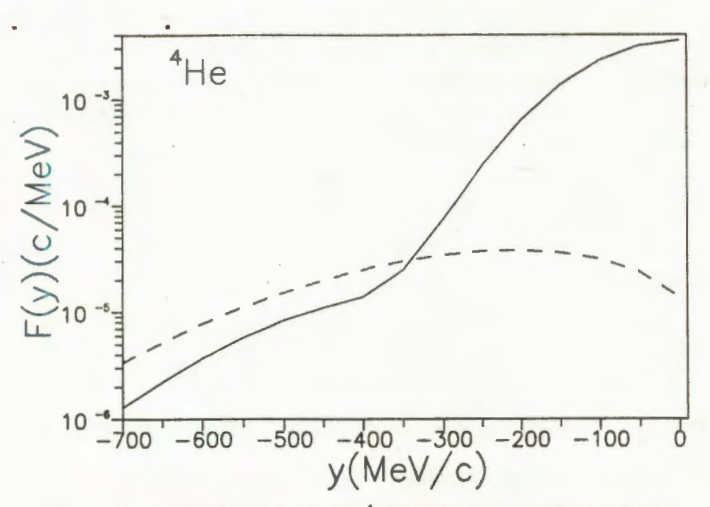


Fig. 1. The scaling function F(y) of <sup>4</sup>He (solid line) and the function B(y) (dashed line) calculated by using the nucleon momentum distribution n(k) from [13]

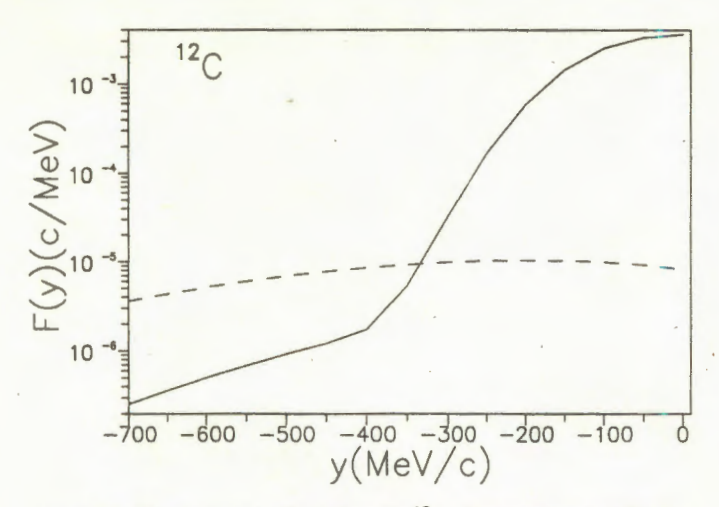


Fig. 2. The same as in Fig. 1, but for <sup>12</sup>C. The nucleon momentum distribution used in the calculation is from [26]

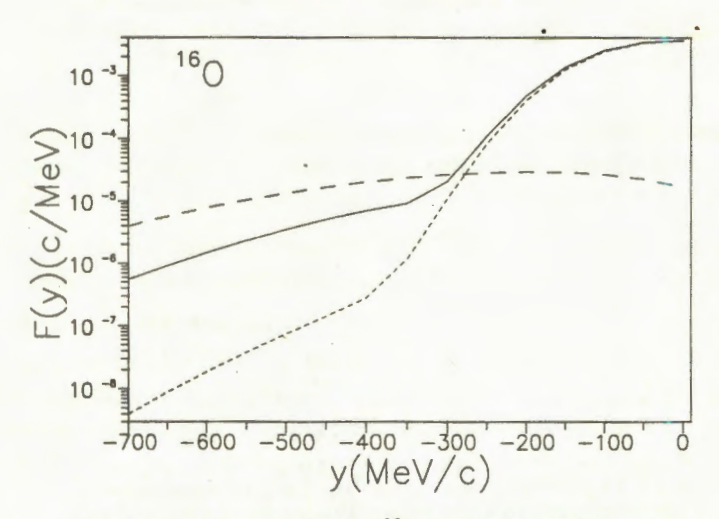


Fig. 3. The scaling function F(y) of <sup>16</sup>O (solid line) and the function B(y) (long-dashed line) calculated by using the nucleon momentum distribution from [12,13]. The short-dashed line is the scaling function F(y) calculated by using n(k) from [15]

large values of |y|. This confirms the conclusions from [8] on the necessity of the electron-nuclei quasielastic cross sections to be calculated in terms of spectral functions and not simply by convoluting the free electron-nucleon cross section with the nucleon momentum distribution.

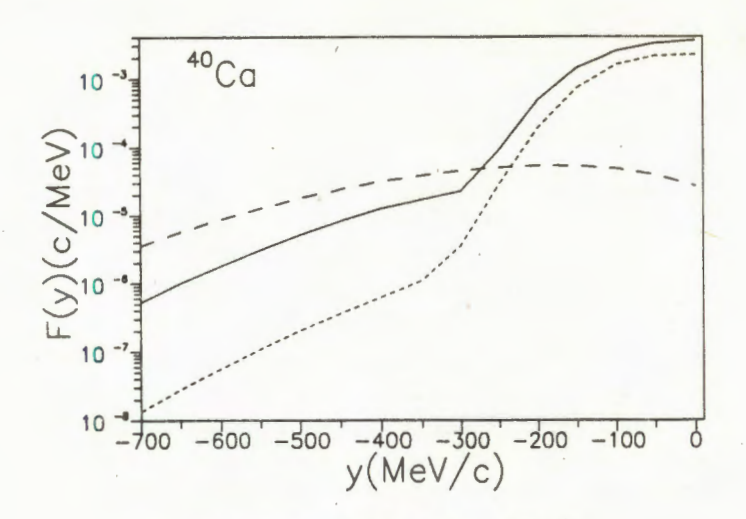


Fig.4. The same as in Fig.3, but for 40 Ca

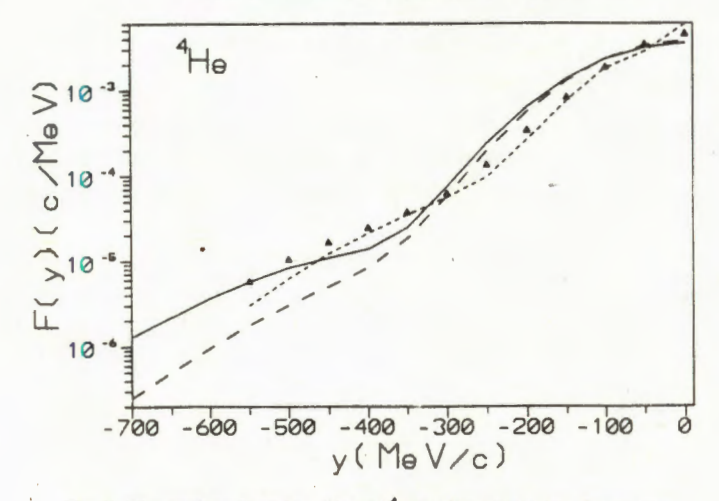


Fig. 5. The scaling function F(y) of <sup>4</sup>He. The solid triangles represent the experimental scaling function from [10]. The results of this work: calculations by using n(k) from [13] (solid line) and calculations by using n(k) from [15] (long-dashed line). The short-dashed line is the result from [10]

The scaling functions F(y) for the <sup>4</sup>He and <sup>12</sup>C nuclei calculated in this work are compared in Figs.5 and 6 with the available experimental data for the asymptotic scaling function. They are compared also with the results of our calculations for the scaling function in <sup>4</sup>He, <sup>16</sup>O and <sup>40</sup>Ca (Figs.3—6)

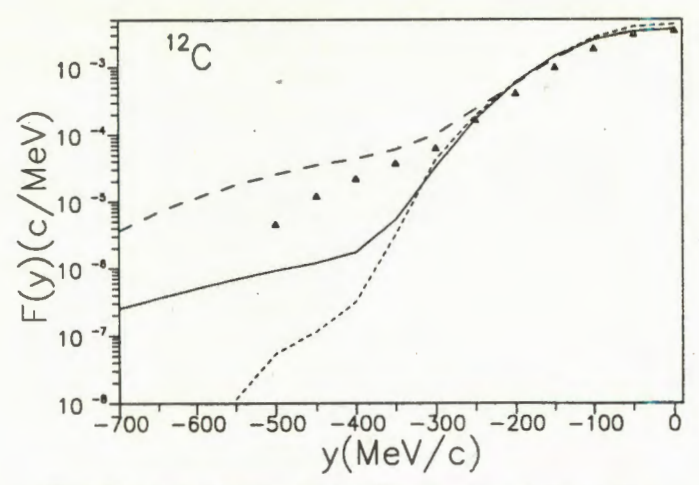


Fig. 6. The scaling function F(y) of <sup>12</sup>C. The solid triangles represent the experimental scaling function from [10]. The result of this work: calculations by using n(k) from [26] (solid line). The long-dashed line is the result from [27]. The short-dashed line is result in the Hartree-Fock method (taken from [7])

using the nucleon momentum distributions from the phenomenological correlation model accounted for short-range and tensor correlations [15]. In this case  $n_{\rm ex}(k)$  is identified with the third terms in the right-hand side of eqs. (10), (11) and (12) in [15] for the <sup>4</sup>He, <sup>16</sup>O and <sup>40</sup>Ca nuclei, correspondingly, while  $n_{\rm gr}(k)$  is identified with the sum of all other terms in the right-hand side of the same equations.

In the case of <sup>4</sup>He and <sup>12</sup>C the scaling functions calculated in [7] and [10] using many-body correlated wave functions from [27] are given in Figs.5 and 6, respectively. The predictions of the Hartree-Fock method (taken from [7]) are shown in Fig.6 for the case of the <sup>12</sup>C nucleus.

It can be seen from Fig.5 that the scaling function F(y) for <sup>4</sup>He calculated within the JCM is in good agreement with the experimental data and with the results from [10]. The same is true for F(y) calculated using the PM from [15] for  $y \ge -350$  MeV/c. The JCM result for F(y) in <sup>12</sup>C is similar to that from the correlation method from [7,10,27] for  $|y| \le 300$  MeV/c. The values of F(y) at |y| > 300 MeV/c are much larger than those obtained in the Hartree-Fock method. This is due to the nucleon correlation effects in the momentum distribution calculated in the Jastrow method. We note the difference between the results for F(y) at |y| > 300 MeV/c obtained in the JCM

and in the PM in the cases of  $^{16}$ O and  $^{40}$ Ca. We emphasize the necessity of obtaining experimental data for F(y) in these nuclei as a test of the various correlation methods.

Table. Mean kinetic ( $\langle T \rangle$ ) and mean removal ( $\langle E \rangle$ ) energies, occupation probabilities  $S_{gr}$  and  $S_{ex}$  calculated within the Hartee-Fock (HF) approximation and in many-body correlation methods [11,12,13,15,28,29,30] and the binding energy per nucleon ( $E_A/A$ )

Nuclei		⟨T⟩ MeV	⟨E⟩ MeV	$S_{\rm gr}$	Sex	E <sub>A</sub> /A [eq.(10)] MeV	$(E_A/A)_{\text{exp}}$ [32] MeV
<sup>4</sup> He	Shell model [28]	17.1	19.8	1.0	0.0	4.20	7.07
	Ref. [28]	21.1	28.2			7.07	
	Ref.[30]	28.7					
	calculated in this work using						
	Ref.[11]	25.96	31.45	0.93	0.07	7.07	
	Ref. [15]	20.35	27.71	0.93	0.07	7.07	
	Ref. [12,13]	25.79	31.34	0.905	0.095	7.07	
<sup>12</sup> C	HF [29]	17.0	23.0	1.0	0.0	3.77	7.68
	Ref. [29]	37.0	49.0	0.8	0.2	7.68	
	calculated in this- work using	-					
	Ref. [26]	20.97	34.42.	0.98	0.02	7.68	
<sup>16</sup> O	HF [29]	15.0	24.0	1.0	0.0	5.00	7.97
	Ref. [29]	27.0	41.0			7.90	
	Ref. [30]	34.4					
	calculated in this work using						
	Ref. [15]	19.73	34.37	0.94	0.06	7.98	
	Ref. [12,13]	21.28	35.81	0.95	0.05	7.97	
<sup>40</sup> Ca	HF [29]	16.5	26.6	1.0	0.0	5.26	8.55
	Ref. [29]	36.0	52.1	0.8	0.2	8.51	
	calculated in this work using						
	Ref. [15]	18.71	.35.33	0.91	0.09	8.55	
	Ref. [12,13]	23.29	39.80	0.91	0.09	8.55	

## 3.2. Mean Kinetic and Mean Removal Energy

The study of the nucleon correlation effects using realistic nucleon-nucleon interactions shows [28-30] a substantial increase of the values of the mean kinetic  $\langle T \rangle$  and mean removal  $\langle E \rangle$  energy with respect to their Hartree-Fock values, as well as a strong relation between the high-momentum components in the momentum distribution. This link is quantitatively explained within the two-nucleon correlation model [31] in which the high-momentum components of a nucleon are generated by its hard interaction with a single nucleon, whereas the remaining (A - 2) nucleons (the soft nucleons) move in the mean field with c.m. momentum  $k_{A-2} \approx 0$ . Eqs. (11—13) allow us to calculate  $\langle T \rangle$  and  $\langle E \rangle$  using the momentum distributions from [11— 15]. We note that  $|\varepsilon_A|$ ,  $\langle T \rangle$  and  $\langle E \rangle$  have to satisfy the Koltun's sum rule (eq. 10)) [16]. The values of the mean kinetic and removal energy, as well as the binding energy per nucleon evaluated by using of eq. (10), which are calculated within the shell model, in the Hartree-Fock method and in various correlation methods for the <sup>4</sup>He, <sup>12</sup>C, <sup>16</sup>O and <sup>40</sup>Ca nuclei are given in the Table. It can be seen that the increase of the values of  $\langle T \rangle$  and  $\langle E \rangle$  due to the correlation effects is quite a general feature of the many-body calculations. The values of  $\langle T \rangle$  and  $\langle E \rangle$  obtained in our correlation approaches give a correct value for the binding energy per nucleon, which is not the case in the shell model and in the Hartree-Fock method. The values of the occupation probabilities  $S_{qq}$  and  $S_{qq}$  are listed also in the Table. They are obtained using eqs.(14) and (15) in calculations for  $^4$ He,  $^{12}$ C,  $^{16}$ O and  $^{40}$ Ca nuclei. Due to the ground state correlations the values of  $S_{\rm gr}$  are less than unity (while  $S_{gr}^{HF} = 1$ ) and the values of  $S_{ex}$  are larger than zero (while  $S_{ex}^{HF} = 0$ ).

## 4. Conclusions

It is shown in the y-scaling method that if only nucleonic degrees of freedom are considered within the framework of the PWIA, then at sufficiently high values of q the structure function F(q, y) becomes a function only of y. The analysis of the y-scaling in the region where it is observed (y < 0) allows one to obtain information on the important characteristics of the nucleon dynamics (e.g., on the nucleon momentum distribution) in nuclei. The analysis in the region where the scaling is not observed (y > 0) yields information on the effects which break down the impulse approximation and shows the limits of the independent-particle description of the nuclear systems.

The main conclusion of the y-scaling analysis is that the experimentally obtained asymptotic scaling function, as well as the scaling function calculated in various correlation methods differ largely from the scaling function obtained in the MFA. The binding correction to the scaling function can be explicitly evaluated using the nuclear spectral function. These conclusions are confirmed in the present work by the calculations of the scaling functions F(y) and the binding correction B(y) by using realistic momentum distributions obtained within the correlation approaches, such as the Jastrow method [12,13] and the phenomenological correlation model [14,15] in the case of the <sup>4</sup>He, <sup>12</sup>C, <sup>16</sup>O and <sup>40</sup>Ca nuclei. The increased calculated values of the mean kinetic  $\langle T \rangle$  and mean removal  $\langle E \rangle$  energy in comparison with the shell-model and the Hartree-Fock calculations lead to correct results for the binding energy per nucleon in the nuclei considered. The values of  $\langle T \rangle$  and (E) obtained in this work can be related to the presence of high-momentum and removal energy components in the many-body spectral function. These values reflect the extent to which the short-range nucleon-nucleon correlations are accounted for in the methods considered in this work.

#### References

- Antonov A.N., Hodgson P.E., Petkov I.Zh. Nucleon Correlations in Nuclei, Springer—Verlag, Berlin—Heidelberg—New-York, 1993.
- 2. West G.B. Phys. Rep., 1975, 18, p.263.
- Ciofi degli Atti C:, Pace E., Salme G. Few Body Systems, Suppl., 1986, 1, p.280.
- 4. Ciofi degli Atti C., Pace E., Salme G. Phys. Rev., 1987, C36, p.1208.
- 5. Ciofi degli Atti C. Nucl. Phys., 1987, A463, p.127c.
- 6. Ciofi degli Atti C., Pace E., Salme G. Phys. Rev., 1989, C39, p.259.
- Ciofi degli Atti C., Pace E., Salme G. Nucl. Phys., 1989, A497, p.361c.
- Ciofi degli Atti C., Pace E., Salme G. Preprint INFN-ISS 90/8, Roma, 1990.
- Ciofi degli Atti C., Pace E., Salme G. Preprint INFN-ISS 87/7, Roma, 1987: Nucl. Phys., 1990, A508, p.349c.
- 10. Ciofi degli Atti C., Pace E., Salme G. Phys. Rev., 1991, C43, p.1155.
- 11. Bohigas O., Stringari S. Phys. Lett., 1980, 95, p.9.
- Stoitsov M.V., Antonov A.N., Dimitrova S.S. Phys. Rev., 1993, C47, p.R455; Phys. Rev., 1993, C48, p.74.
- Stoitsov M.V., Antonov A.N. Z. Phys., 1993, A345, p.259;
   Stoitsov M.V., Antonov A.N., Dimitrova S.S. Z. Phys., 1993, A345, p.359.

- 14. Dellagiacoma F., Orlandini G., Traini M. Nucl. Phys., 1983, A393, p.95.
- 15. Traini M., Orlandini G. Z. Phys., 1985, A321, p.479.
- Koltun D.S. Phys. Rev. Lett., 1972, 28, p.182; Phys. Rev., 1974, C9, p.484.
- 17. Day D.B. et al. Phys. Rev. Lett., 1979, 43, p.1143.
- 18. Rock S. et al. Phys. Rev., 1982, C26, p.1592.
- 19. Day D.B. et al. Phys. Rev. Lett., 1987, 59, p.427.
- 20. Day D.B. et al. Phys. Rev., 1989, C40, p.1011.
- Ciofi degli Atti C. et al. In: Proceedings of the 4th Workshop on Perspectives in Nuclear Physics at Intermediate Energies, Trieste, 8—12 May 1989, Ed. S.Boffi, C.Ciofi degli Atti, Giannini M., World Scientific Publ. Co., Singapore, 1989, p.312.
- 22. Ciofi degli Atti C., Liuti S., Simula S. Phys. Rev., 1990, C41, p.R2474.
- 23. Jastrow R. Phys. Rev., 1955, 98, p.1479.
- 24. Gaudin M., Gillespie J., Pipka G. Nucl. Phys., 1971, A176, p.237.
- 25. Dal Ri M., Stringari S., Bohigas O. Nucl. Phys., 1982, A376, p.81.
- Stoitsov M.V., Anotonov A.N., Dimitrova S.S. In: Proceedings of the 6th Workshop on Perspectives in Nuclear Physics at Intermediate Energies, Trieste 3—7 May 1993, Ed. S.Boffi, C.Ciofi degli Atti, M.Giannini, World Scientific Publ. Co., Singapore (in print).
- 27. Benhar O. et al. Phys. Lett., 1986, 177B, p.135.
- 28. Ciofi degli Atti C., Liuti S. Phys. Rev., 1990, C41, p.1100.
- 29. Ciofi degli Atti C., Liuti S. Phys. Rev., 1989, 225B, p.215.
- 30. Pieper S.C., Wiringa R.B., Pandharipande V.R. Phys. Rev., 1992, C46, p.1741.
- 31. Frankfurt L., Strikman M. Phys. Rep., 1981, 76, p.215; Phys. Rep., 1988, 160, p.236.
- 32. Kravtsov V.A. Atomic Masses and Nuclear Binding Energies, Moscow, Atomizdat, 1974.